Universidade de Lisboa

Faculdade de Farmácia


# Development of lipid-polymer hybrid nanoparticles as a strategy to treat Alzheimer's Disease

Catarina Cachão Roque

Dissertation supervised by Doctor Paula Soares and co-supervised by Professor António Almeida

Master in Biopharmaceutical Sciences

2022

Universidade de Lisboa

Faculdade de Farmácia


# Development of lipid-polymer hybrid nanoparticles as a strategy to treat Alzheimer's Disease

Catarina Cachão Roque

Dissertation supervised by Doctor Paula Soares and co-supervised by Professor António Almeida

Master in Biopharmaceutical Sciences

2022

# Acknowledgments

Em primeiro lugar, quero agradecer à minha orientadora, Doutora Paula Soares, por toda a ajuda, colaboração e disponibilidade durante todo o desenvolvimento da tese. Ainda que o processo não tenha acontecido tal como idealizado, a vontade em prestar auxílio esteve sempre presente, acima de tudo nunca me deixou sentir desamparada.

Ao meu coorientador, Professor Doutor António Almeida, por me ter permitido integrar o seu grupo de investigação.

À Professora Lídia, que tentou sempre ajudar no desenvolvimento do nanossistema, em especial na sua otimização.

Um obrigada muito especial à Catarina, que foi incansável durante todo o ano. Fizeste o que podias e o que não podias, tornaste tudo o que foi feito possível. Para além disso, foste a primeira a dar-me força para acreditar em mim e num futuro como cientista desde o projeto de licenciatura. Foste, durante este último ano conselheira e ombro amigo, e por isso só te tenho a agradecer por tudo.

À minha família, pais, irmão e avós, por terem sido sempre o porto de abrigo nos dias menos bons, e por terem sempre celebrado as minhas vitórias. A vocês, não só vos devo a vida como tudo o que sou hoje.

Um grande obrigada também a todo o pessoal do laboratório de polímeros, em especial à Adriana que foi sempre um amor! Obrigada por toda a compreensão e pelos desabafos, és uma pessoa linda!

À Rita, que é amiga desde a licenciatura, foi colega de mestrado e é companheira de vida! Obrigada, amiga, por tudo o que aturaste e aturas, e obrigada pela paciência. És uma pessoa muito importante na minha vida, e espero que seja sempre assim.

Por fim, mas não menos importante, o meu muito obrigada a todo o grupo Membrane Traffic in Disease. Em especial, ao Professor Duarte Barral e à Cristina, por me terem dado oportunidade de aprender mais sobre as suas áreas. Ao Luís e ao Charneca, obrigada por me terem aturado todos os dias! Trouxeram um ânimo à minha vida que há muito não existia, acho que não têm noção da importância que tiveram em todo o processo, mas foram elementos cruciais. Espero levar-vos para a vida.

A todos, o meu muito obrigada.

# Resumo

A doença de Alzheimer (AD) é uma doença neurodegenerativa crónica responsável pela maioria dos casos de demência no mundo. Apesar da grande incidência da AD na população mundial, ainda não existe uma abordagem de tratamento eficaz para a patologia. A terapia farmacológica que existe para a doença de AD apenas trata os sintomas, não sendo capaz de induzir ou prevenir regressão da doença.

Devido aos muitos fatores que estão envolvidos na patologia da AD, uma terapia de múltiplos alvos seria a ideal para esta patologia. Isto, aliado ao facto de a AD ser uma doença do sistema nervoso central (CNS) e de o CNS estar protegido por uma barreira altamente seletiva, a barreira hematoencefálica (BBB), explica a ausência de um tratamento eficaz da doença.

Outra limitação para tratar a perturbação é a falta de um diagnóstico preciso. No passado, um diagnóstico preciso desta patologia era mais difícil. No entanto, hoje em dia o uso de técnicas de neuroimagem como a ressonância magnética (MRI) podem dar importantes informações sobre biomarcadores.

Devido a todas as limitações existentes para criar um tratamento eficaz e local da AD, esta tese de mestrado propõe o desenvolvimento de um nanossistema composto por nanopartículas híbridas de tamanho suficientemente pequeno para passar pelo BBB, que encapsulam, por sua vez, nanopartículas superparamagnéticas de óxidos de ferro (SPIONs) e um fármaco (curcumina). O nanossistema incluirá também a funcionalização destas nanopartículas com um péptido penetrante de células (CPP) que permite a translocação de membranas celulares.

O nanossistema proposto pode ser considerado um agente de teranóstico, uma vez que é capaz de ter tanto um efeito terapêutico como de diagnóstico na AD. O efeito terapêutico é dado pela curcumina presente nas nanopartículas, e o efeito de diagnóstico é dado pelas SPIONs encapsuladas uma vez que podem atuar como agentes de contraste para ressonância magnética, permitindo o diagnóstico da AD.

Todas as nanopartículas foram caracterizadas durante as diferentes fases do trabalho. As SPIONs produzidas foram analisadas por microscopia eletrónica de transmissão e o tamanho médio obtido foi de 12,3 ± 2,3 nm. Em seguida, todas as nanopartículas produzidas durante a otimização das nanopartículas híbridas foram caracterizadas utilizando a técnica DLS. Os diâmetros hidrodinâmicos obtidos para as nanopartículas não funcionalizadas foram de 91,6 ± 1,6 nm e para o nanossistema final (funcionalizado) foram de 120,1± 0,1 nm.

Para avaliar a eficiência de internalização das nanopartículas nas células, foi utilizada uma linha celular de células endoteliais humanas do cérebro. A mesma linha celular foi também

utilizada para realizar ensaios de citotoxicidade. Os ensaios celulares mostraram que as nanopartículas conseguem internalizar nas células, sendo que o nanossistema mostrou uma capacidade de internalização mais elevada do que as nanopartículas híbridas + SPIONs. Os dois tipos de nanopartículas testados também mostraram uma tendência para se tornarem citotóxicos nas concentrações testadas mais elevadas.

As características do nanossistema produzido nesta tese de mestrado mostram-se promissoras para atravessar a BBB devido à sua capacidade de internalização numa linha celular de células endoteliais do cérebro humano *in vitro*.

**Palavras-chave:** Doença de Alzheimer; Barreira hematoencefálica; Péptido penetrante de celular; SPIONs; Nanopartículas híbridas

# Abstract

Alzheimer's disease (AD) is a chronic neurodegenerative disorder responsible for most cases of dementia in the world. Despite the large incidence of AD in the world population, there is still no effective treatment approach to the pathology. The pharmacologic therapy that exists for AD only treat the symptoms, it is not able to induce or prevent disease regression.

Due to the many factors that are involved in AD pathology, a multiple-target therapy would be the preferred treatment for this pathology. This, allied to the fact that AD is a central nervous system (CNS) disorder and that the CNS is protected by a highly selective barrier, the blood-brain barrier (BBB), explains the absence of effective treatment for the disorder.

Another limitation in treating the disorder is the lack of an accurate diagnosis. In the past, an accurate diagnosis of this pathology was more difficult. Nowadays the use of neuroimaging techniques such as magnetic resonance imaging (MRI) can give important biomarker information.

Due to all the existing limitations to creating an effective and local treatment for AD, this master thesis proposes the development of a nanosystem composed of hybrid nanoparticles with a small enough size to pass through the BBB, that encapsulates superparamagnetic iron oxide nanoparticles (SPIONs) and a drug (curcumin). The nanosystem will also include the functionalization of these nanoparticles with a cell-penetrating peptide (CPP) that allows the translocation of cell membranes.

The proposed nanosystem can be considered a theranostics agent, since it is able to both have a therapeutic and diagnostic effect on AD. The therapeutic effect is given by the curcumin present in the nanoparticles, and the diagnostic effect is given by the SPIONs encapsulated since they can act as contrast agents in MRI, allowing AD diagnosis.

All nanoparticles were characterized during the different stages of the work. The produced SPIONs were analyzed by transmission electron microscopy and the obtained average size was $12.3 \pm 2.3$ nm. Then, all the nanoparticles produced during the optimization of the hybrid nanoparticles were characterized using DLS technique. The hydrodynamic diameters obtained for the nanoparticles not functionalized was $91.6 \pm 1.6$ nm and for the final nanosystem (functionalized) was $120.1 \pm 0.1$ nm.

To assess the efficiency of the nanoparticles in internalizing in cells, a cell line of human brain endothelial cells was used. The same cell line was also used to perform cytotoxicity assays. Cellular assays showed that the nanoparticles can internalize in the cells. However, the nanosystem showed a higher internalization capacity when compared to the hybrid nanoparticles + SPIONs. Both types of nanoparticles tested also showed a tendency to become cytotoxic at the higher concentrations tested.

The characteristics of the produced nanosystem in this master thesis are promising to overcome the BBB due to their ability to internalize in a cell line of human brain endothelial cells *in vitro*.

**Keywords:** Alzheimer's Disease; BBB; CPP; SPIONs; Hybrid nanoparticles

# Contents

# List of Figures

# List of Tables

# List of Abbreviations

| | |
|---|---|
| **Aβ** | Amyloid-β |
| **AD** | Alzheimer's Disease |
| **APP** | Amyloid Precursor Protein |
| **ATR** | Attenuated Total Reflectance |
| **BBB** | Blood-Brain Barrier |
| **CNS** | Central Nervous System |
| **CPP** | Cell Penetrating Peptide |
| **DCM** | Dichloromethane |
| **DL** | Drug Loading |
| **DLS** | Dynamic Light Scattering |
| **DMF** | Dimethylformamide |
| **EDC** | N-ethyl-N′-(3-(dimethylamino)propyl)carbodiimide |
| **EE** | Encapsulation Efficiency |
| **FDA** | Food and Drug Administration |
| **FTIR** | Fourier Transform Infrared |
| **LPHNPs** | Lipid-Polymer Hybrid Nanoparticles |
| **MRI** | Magnetic Resonance Imaging |
| **NFTs** | Neurofibrillary Tangles |
| **NHS** | N-Hydroxysuccinimide |
| **PEG** | Polyethylene Glycol |
| **PET** | Positron Emission Tomography |
| **PI** | Polydispersity Index |

| | |
|---|---|
| **PLA** | Polylactic Acid |
| **PLGA** | Polylactic-co-glycolic Acid |
| **PNPs** | Polymeric Nanoparticles |
| **SC** | Sodium Cholate |
| **SD** | Sodium Deoxycholate |
| **SPIONs** | Superparamagnetic Iron Oxide Nanoparticles |
| **SQUID** | Superconducting Quantum Interference Device |
| **TEM** | Transmission Electron Microscopy |
| **THF** | Tetrahydrofuran |
| **TJs** | Tight Junctions |
| **XRD** | X-ray Diffraction |

# Chapter 1

# General Introduction

## 1. Alzheimer's disease

Alzheimer's disease (AD) is a chronic neurodegenerative disorder responsible for most cases of dementia in the world**.** This pathology is characterized by rapid growth affecting mainly the elderly population, thus making age a risk factor for developing the disease (Shabbir et al., 2021). Mutations in genes coding for amyloid precursor protein (APP) can also constitute a risk factor for AD although it only causes 5% of all AD cases (Chin et al., 2013).

The symptoms that better characterize this pathology are dementia, memory loss and changes in cognitive and motor performances (Bhat et al., 2019).

The amyloid cascade hypothesis is the prevalent hypothesis to explain the mechanism of AD. However, AD is a complex disease that results from multiple factors rather than a single cause. This way, it cannot be fully explained by the amyloid cascade hypothesis since the major hallmarks of the disease are extracellular amyloid plaques, intracellular neurofibrillary tangles (NFTs) and neuroinflammation (Chin et al., 2013; Lane et al., 2018). These events are followed by neuronal cell death.

### 1.1. Amyloid Cascade Hypothesis

The amyloid cascade hypothesis explains the formation of amyloid-β (Aβ) by cleavage of the APP by different secretases. The APP is a type 1 transmembrane protein highly abundant in the central nervous system (CNS). There, the APP can be metabolized following two different pathways: the non-amyloidogenic pathway and the amyloidogenic pathway (De-Paula et al., 2012; Soria Lopez et al., 2019). In the non-amyloidogenic pathway, the APP is cleaved by α-secretase resulting in two products: an N-terminal fragment named sAPPα (soluble extracellular product) and a C-terminal fragment with 83 amino acids (C83) that remains bound

to the membrane. Then, the C83 is cleaved by γ-secretase and that generates a 3kDa product named p3 which is the last product of the non-amyloidogenic pathway (Soria Lopez et al., 2019).

In contrast to non-amyloidogenic pathway, the amyloidogenic pathway starts with the cleavage of APP not by the α-secretase but β-secretase. The result of this cleavage is an N-terminal fragment named sAPPβ and a C-terminal fragment with 99 amino acids (C99) that remains bound to the membrane, similar to C83 in non-amyloidogenic pathway, C99 is then cleaved by γ-secretase and the result product is Aβ (De-Paula et al., 2012).

C83 and C99 differ in 16 amino acids in their length, which is enough for C83 does not contain the entire amyloidogenic amino acid sequence and C99 does, as seen in Figure 1.1. The resultant Aβ from the amyloidogenic pathway can mainly be constituted by 40 amino acids ($A\beta_{40}$) or 42 amino acids ($A\beta_{42}$) and they are released as native monomers (Lane et al., 2018).

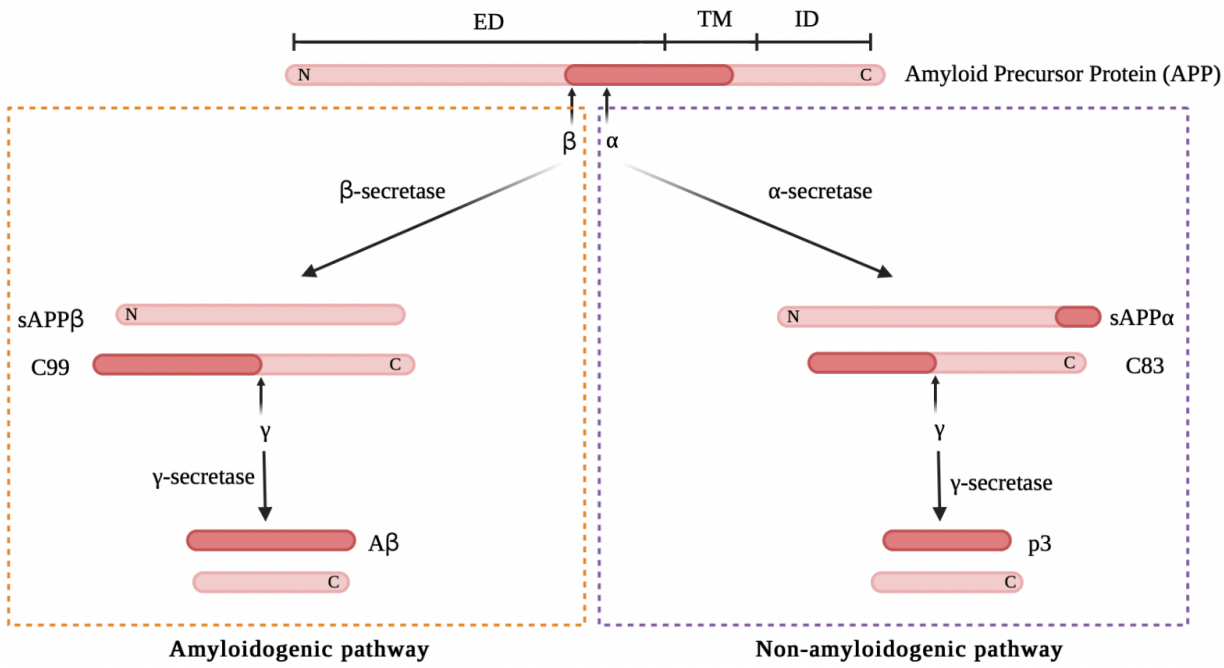


**Figure 1.1** Schematic representation of APP metabolization through amyloidogenic pathway and non-amyloidogenic pathway. Adapted from (H. Zheng & Koo, 2006).

Both amyloidogenic and non-amyloidogenic pathways occur in healthy individuals. This way, Aβ monomers are produced not only under pathological conditions but also in healthy individuals (Chin et al., 2013). The main difference between both cases is the fact that in a patient with the pathology there is an imbalance between Aβ production and clearance. This way, *in vivo* concentrations of the monomers start to increase, and the monomers self-aggregate. They can acquire different structures until they reach the Aβ plaques form, being the most

neurotoxic ones the intermediate soluble Aβ oligomers (Farkhondeh et al., 2019; Hane et al., 2017).

When the Aβ oligomers start being produced, they will be able to interact with CNS cells, such as neurons and glial cells inducing, this way, downstream events. These events include neuroinflammation (elevated expression of proinflammatory cytokines) and hyperphosphorylation of Tau protein (Soria Lopez et al., 2019).

Tau protein is widely expressed in the CNS. It is normally soluble and plays an important role in keeping microtubules stable. However when it is hyperphosphorylated it becomes insoluble and starts aggregating and forming the NFTs (Querfurth & Laferla, 2010). NFTs play such an important role in AD since there is evidence that solely the presence of Aβ plaques is not enough to induce AD symptoms to the patient. This way, for AD diagnosis both Aβ plaques and NFTs presence is required (Lane et al., 2018). Moreover, there is already evidence that an immunotherapy approach to remove Aβ plaques does not prevent further neurodegeneration (Chin et al., 2013).

## 1.2. Diagnosis of AD

The diagnosis of AD has been improving with the development of new technologies, namely non-invasive neuroimaging techniques (Ausó et al., 2020). Ideally, AD diagnosis should occur in the early stages of the disease since the current therapies are not able to revert already existing symptoms. However, what usually happens is a diagnosis at a mild to moderate stage of the disease (Chen et al., 2018).

In the past, an accurate diagnosis of this pathology was very difficult since the diagnosis was made by exclusion of other pathologies (Porsteinsson et al., 2021). Nowadays, important biomarker information can be obtained by neuroimaging techniques such as magnetic resonance imaging (MRI) and positron emission tomography (PET). Both techniques allow the detection of diagnostic biomarkers in pre-symptomatic patients being the most accurate PET (Wolinsky et al., 2018).

Another way to search for important biomarkers is by analysis of cerebrospinal fluid samples. This type of analysis can detect the presence of hyperphosphorylated Tau and Aβ plaques (Wolinsky et al., 2018).

## 1.3. Current therapeutical approaches

Despite the large incidence of AD in the world population, there is still no effective treatment approach to the pathology. Currently, there are only two classes of pharmacologic therapy for AD, being the cholinesterase inhibitors (Donepezil®, Rivastigmine® and Galantamine®) and a glutamate antagonist (Memantine®) (Scheltens et al., 2016). The main problem related to these inhibitors is the fact that they only treat the symptoms, they are not able to prevent or induce disease regression (Weller & Budson, 2018).

Due to the many factors that are involved in AD pathology, a multiple-target therapy would be the preferred treatment for this pathology (Chen et al., 2018). According to the amyloid cascade hypothesis, to efficiently treat AD the main targets are Aβ plaques and NFTs. An important compound that has been described to have multi-targeted effects on AD is curcumin.

### 1.3.1. Curcumin

Curcumin is a natural polyphenolic compound that has been widely studied due to its various pharmacological activities (Farkhondeh et al., 2019). This compound is known for having a significant role in neurodegenerative diseases, such as AD. Its structure can be seen in Figure 1.2.

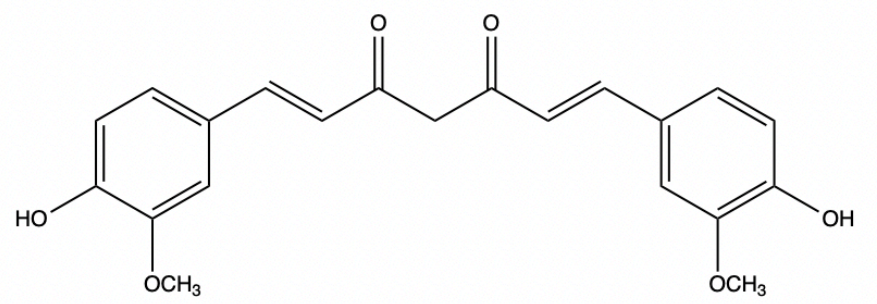


**Figure 1.2** Chemical structure of curcumin

Curcumin exhibits many properties, including antioxidant, anti-inflammatory, and neuroprotective (Fan et al., 2018). Due to its large properties, curcumin is able to target many different pathways (Farkhondeh et al., 2019). However, there are some limitations related to the use of this compound since it is poorly soluble in water, has a rapid clearance , is poorly absorbed and consequently has a low bioavailability (especially when administered orally) (Yavarpour-Bali et al., 2019).

The use of curcumin in humans has already been investigated and it is known to be safe, even at high doses of up to 8 g per day (Farkhondeh et al., 2019; Shabbir et al., 2021)

The anti-inflammatory property of curcumin allows it to bind to Aβ and prevent protein aggregation, avoiding the formation of neurotoxic species (Bhat et al., 2019). It can also promote a decrease in the production of Aβ, the hyperphosphorylation of Tau protein and, consequently, the formation of NFTs (Fan et al., 2018). There are already *in vitro* studies suggesting that curcumin decreases the production of Aβ by attenuating APP maturation ( Chen et al., 2018).

Besides the anti-inflammatory properties of curcumin, the antioxidant property is also very important in AD, since it is already confirmed that reactive oxygen species play an important role in AD pathogenesis (Bhat et al., 2019).

To play a significant role in AD, curcumin must cross the blood-brain barrier (BBB) and reach the CNS. Even though curcumin has a low molecular weight, there are some limitations to the accumulation of this compound in the brain since this compound has a limited permeability through the barrier. For instance, an intravenous administration leads to a detectable amount of curcumin in the brain while an oral administration does not (Chin et al., 2013). It is also already reported that administration of polylactic-co-glycolic acid (PLGA) nanoparticles encapsulating curcumin leads to higher concentrations of curcumin in the brain and a higher bioavailability when compared to administration of conventional curcumin (Bhat et al., 2019; Fan et al., 2018; Farkhondeh et al., 2019).

Another important feature of curcumin is its photophysical and photochemical properties due to its structure. When curcumin binds to Aβ plaques emits fluorescence, which can turn curcumin in an important ally in AD diagnosis (Chen et al., 2018).

# 2. Blood-Brain Barrier

The CNS requires highly specific physiological conditions to allow a proper function of the neurons and to assure an optimal synaptic signaling function (Abbott et al., 2010). To assure the required conditions, there is an interface that separates the CNS from the blood circulation called the blood-brain barrier. The BBB is a selective barrier located at the level of cerebral capillaries capable of allowing or restricting the passage of different substances depending on the CNS needs and thus maintaining the CNS homeostasis (Lowery & Yu, 2017; Obermeier et al., 2016).

The BBB is composed of endothelial cells, pericytes and astrocytes end-feet. Another component of BBB is the basement membrane (BM) that separates the endothelial cells from

the other cellular components (Obermeier et al., 2016). The structure of BBB can be seen in Figure 2.1.

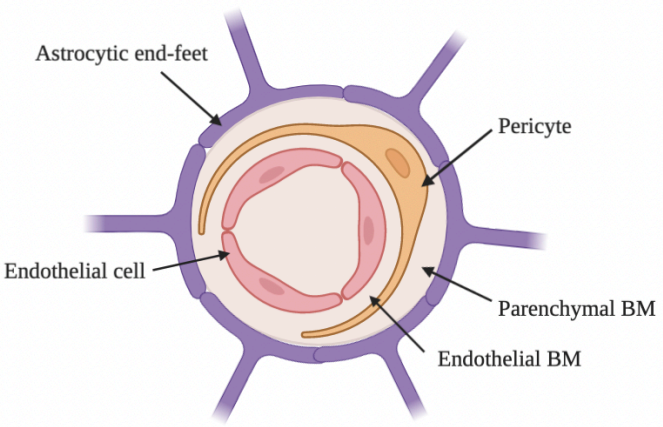


**Figure 2.1** Schematic representation of the blood-brain barrier. Adapted from (Abbott et al., 2010)

Endothelial cells are the basis of BBB; they are interconnected by tight junctions (TJs) forming a cell layer that lines the blood vessels (Fazakas et al., 2011; Sweeney et al., 2018). TJs consist of a complex of proteins including occludin, claudins (1, 3 5 and 12), zona occludens (1, 2 and 3) and junctional adhesion molecules (Sweeney et al., 2018). TJs are the major responsible for the BBB high selectivity (Wilhelm et al., 2013).

In BBB structure, pericytes are embedded in the basement membrane and are in close contact with endothelial cells, being responsible for supporting them. Pericytes are also responsible for controlling cerebral blood flow by controlling the vessels diameter. The pericyte-endothelial interactions lead to the secretion of components of BM (Kircher et al., 2016; Lowery & Yu, 2017; Wilhelm et al., 2013).

BM, the acellular component of BBB, is a specialized extracellular matrix mainly composed of different proteins such as collagen type IV, fibronectin, laminin, and proteoglycans (Wilhelm et al., 2013). The BM can be separated in two different layers, one of them that is produced by endothelial cells and pericytes and the other one that is produced by astrocytes (Profaci et al., 2020).

Finally, astrocytes are responsible for forming the BBB outer layer with their astrocytic end-feet. This cell type expresses glucose transporters, responsible for transporting the glucose into the brain, and other proteins such as P-glycoprotein (Lowery & Yu, 2017; Wilhelm et al., 2013).

Although neither neurons nor microglia cells are present in BBB structure, they play a critical role in BBB regulation. The main purpose of BBB is to provide the ideal environment for neurons so they can work properly. This way any alteration in BBB directly impacts neuron's function. Microglia are the innate immune cells of the CNS that, in the presence of

neuroinflammation, can activate endothelial cells leading to BBB dysregulation (Obermeier et al., 2016).

All BBB components, including neurons and microglia cells form the neurovascular unit. This concept shows the need for a proper function of all involved cells due to their constant cell-cell interactions (Luissint et al., 2012).

## 2.1. Transport across the barrier

Due to its structure, the BBB can limit the passive diffusion of polar substances from the blood to the CNS. This feature also enables the passage of drugs through the barrier impeding their delivery to the brain (Luissint et al., 2012).

Endothelial cells possess two transporters at their surface, being them efflux and solute transporters. Efflux transporters allow the transport of substances up their concentration back to the blood (potentially harmful molecules), while substrate transporters allow the transport of substrates down their concentrations as is the case of glucose (Lowery & Yu, 2017; Profaci et al., 2020) The tight junctions are responsible for decreasing the permeation of polar solutes trough BBB by a diffusional pathway (Abbott et al., 2010; Lowery & Yu, 2017).

Not all compounds are impeded from crossing the BBB. Key factors that make the compounds unable to cross the BBB are a high polar surface area, the ability to form many hydrogen bonds (more than six) and a high molecular weight (Abbott et al., 2010; Pardridge, 2005).

A more recent approach to deliver drugs into the CNS that cannot freely cross the BBB has been to encapsulate them in nanoparticles. However, these nanoparticles can acquire different types of transport, as schematized in Figure 2.2.

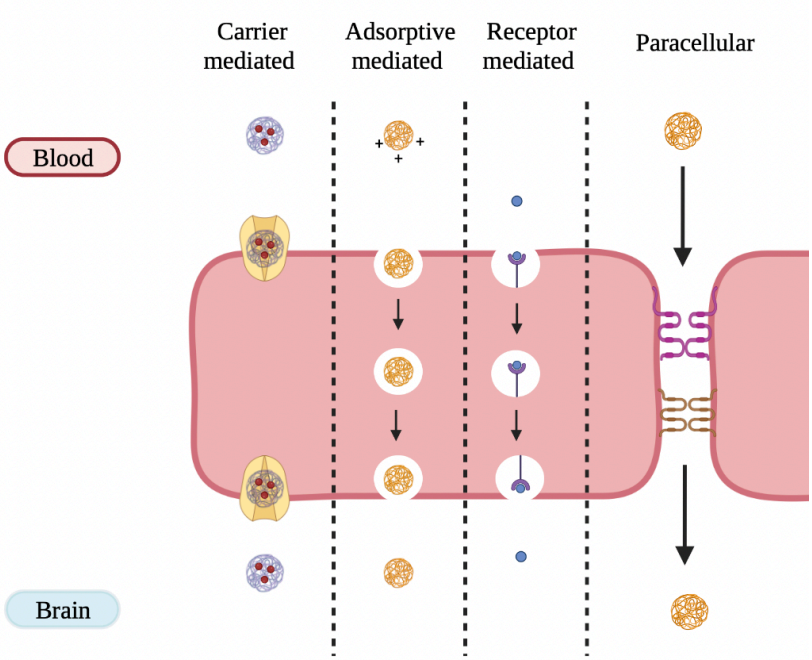


**Figure 2.2** Schematic representation of the different types of transport that the nanoparticles can undergo. Adapted from (Hersh et al., 2022).

Different approaches can be used to modify the nanoparticles surface and ease their way through BBB. They can be modified to target a specific receptor and have a receptor-mediated transport, to follow the adsorptive-mediated transport when positively charged, to be able to diffuse across the barrier by adding lipid molecules to their surface, among others (Hersh et al., 2022). Different types of peptides have been widely used to functionalize nanoparticle's surface and promote their cellular internalization.

## 2.2. Cell Penetrating Peptide

Recently it was discovered that some peptides can translocate cell membranes, named cell penetrating peptides (CPP). These peptides are characterized by having short sequences (less than thirty amino acid residues), being low cytotoxic to cells, and positively charged due to their high basic amino acid residues content. CPPs can translocate into many cells types through an endocytic pathway (Almeida & Vale, 2022; Silva et al., 2019; Vale et al., 2020).

The use of a CPP to modify the nanoparticle's surface is a promising approach since these peptides are able to cross the BBB (Vale et al., 2020). A study already demonstrated that functionalizing the nanoparticle's surface with the CPP K16ApoE significantly increase cell and brain internalization (*in vivo* and *in vitro*) (Ahlschwede et al., 2019).

A CPP that is expected to have a similar effect to K16ApoE is the NV1 CPP. This is a CPP composed of 10 amino acid residues (GFLGWVPTLK).

# 3. Nanosystem

Nanoscale drug carriers have generated a huge interest in the last decades mainly due to their ability for drug delivery. They are also very versatile since a single nanocarrier can acquire both capabilities to imaging diagnostic and therapeutic effect having this way an important role as theranostic agents (Yoon et al., 2012).

These carriers can deliver drugs, nucleic acids and peptides. Their surface can be modified in order to increase their site specificity allowing a targeted delivery and immune system evasion (Cheow & Hadinoto, 2011; Dave et al., 2019). This nanotechnological approach improves the therapeutic efficacy of the drug molecule without any alteration to its structure (Bose et al., 2016). Thus, it allows the delivery of multiple drugs with different properties that can act in different pathologies (Su et al., 2013).

An important parameter to take in account is the size of the nanoparticles, especially when the focus is to cross the BBB. For that purpose, the nanoparticles should not exceed 200 nm (Tsou et al., 2017).

Another important property of nanoparticles is their zeta potential, which indicates the superficial electric charge of the nanoparticles in a colloidal suspension. This value is pH dependent and should be lower than -25 mV or higher than +25 mV to avoid particle aggregation (de Lima & Mortari, 2022).

## 3.1. Superparamagnetic Iron Oxide nanoparticles

Superparamagnetic iron oxide nanoparticles (SPIONs) are small particles usually constituted by $\gamma$-$Fe_2O_3$ (maghemite) or $Fe_3O_4$ (magnetite) that can be coated by organic or inorganic compounds to acquire colloidal stability. They have been widely studied due to their biocompatibility, low toxicity, and superparamagnetic properties (Dulińska-Litewka et al., 2019; Miguel et al., 2020).

SPIONs can be considered theranostic agents, since the same nanoparticle can be used for both therapeutic and diagnostic purposes (Wahajuddin & Arora, 2012).

### 3.1.1. Magnetic properties

Materials can be classified into different types of magnetism, being them superparamagnetism, ferromagnetism, paramagnetism, and diamagnetism.

As can be seen in Figure 3.1, the different types of magnetism acquire different behaviors when an applied magnetic field is applied, obtaining this way, each one of them a characteristic hysteresis curve. The hysteresis curves can be obtained by applying a variable magnetic field and measuring the magnetization value that occurs during the variation of the magnetic field.

The hysteresis curves of each type of magnetism give information about the saturation magnetization (the point where the particle cannot be magnetized any further, in both directions, because the spins are all aligned), coercivity (field required to bring the magnetism to zero) and remanence (residual magnetization) (Nelson et al., 2020; Wahajuddin & Arora, 2012; Wallyn et al., 2019).

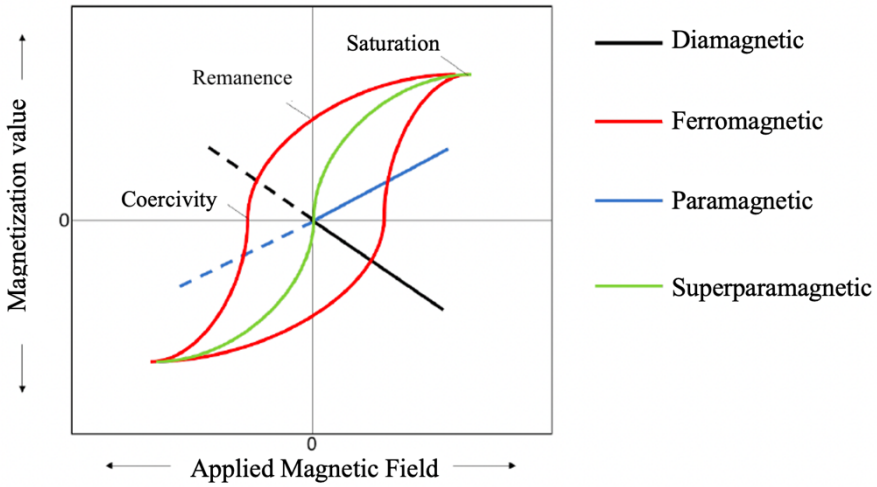


**Figure 3.1** Hysteresis curve of diamagnetic, ferromagnetic, paramagnetic, and superparamagnetic nanoparticles. Adapted from (Nelson et al., 2020).

The nanoparticles that exhibit the superparamagnetism phenomenon only show magnetic interaction when a magnetic field is applied; when it is removed, they no longer show any magnetic interaction (Neuberger et al., 2005). This way, these particles never show any residual magnetic interaction, an important feature for their biological usability (Wahajuddin & Arora, 2012). In this case, both values of coercivity and remanence are 0.

Superparamagnetism is a size-dependent parameter, so for iron oxide nanoparticles to be considered superparamagnetic and called SPIONs it is required that their size do not exceed the 15 nm (Dulińska-Litewka et al., 2019). In Figure 3.2. it is possible to see that SPIONs, at such

small size, do not possess multi domains but a single magnetic domain with high magnetic susceptibility and rapid response to a magnetic field (Abdel Aziz et al., 2020).

Also, in Figure 3.2, it is possible to conclude the same that superparamagnetism is associated with zero coercivity.

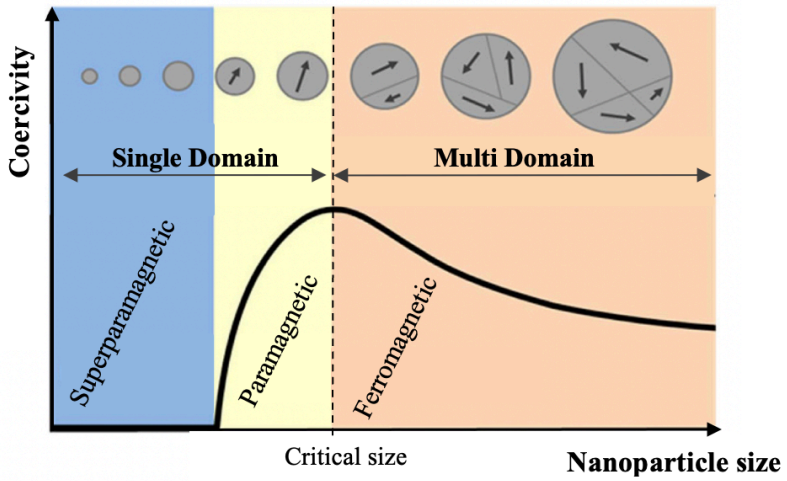


**Figure 3.2** Schematic illustration of the relationship between coercivity, nanoparticles size and magnetic domain structures. Adapted from (Lee et al., 2015).

The superparamagnetism behavior is also dependent on temperature. The transition temperature in which the nanoparticles become superparamagnetic is the blocking temperature ($T_B$) (Jun et al., 2008).$T_B$ can be defined by **Equation 3.1**.

$$K = 25k_B \frac{T_B}{V} \qquad \textbf{Equation 3.1}$$

Where K is the magnetic anisotropy constant, $k_B$ is the Boltzman constant, and V is the volume of a single nanoparticle.

This $T_B$ is responsible for separating two magnetic regimes, the blocked state regime and the superparamagnetic regime. This way, below the $T_B$ the nanoparticles are in a blocked state regime, becoming superparamagnetic above the $T_B$, i.e. when the energy barrier overcome the thermal energy (Wallyn et al., 2019).

The $T_B$ is also size dependent because as it is possible to see in Figure 3.3, the smaller the particle, the easier the nanoparticle to overcome the thermal energy.

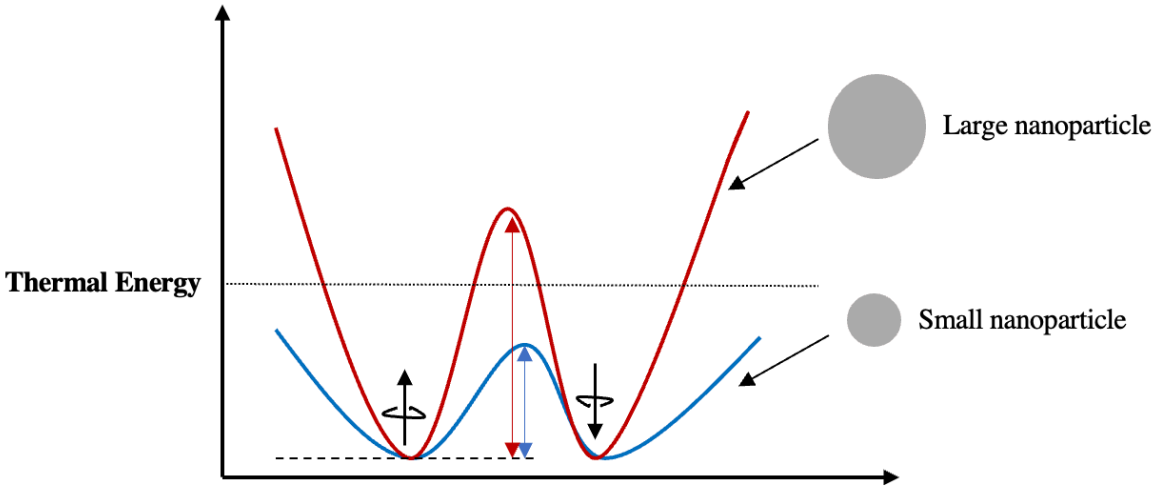


**Figure 3.3** Energy diagram of magnetic nanoparticles with different sizes. Adapted from (Jun et al., 2008)

### 3.1.2. Synthesis of SPIONs

Different techniques can be used to synthesize SPIONs such as co-precipitation, thermal decomposition, hydrothermal, sol-gel, microemulsion, among others (Dadfar et al., 2019). Thermal decomposition and co-precipitation are the preferred techniques to produce SPIONs due to their suitable potential for a large-scale production (Sharifi et al., 2012; Wallyn et al., 2019).

#### 3.1.2.1. Thermal Decomposition

The thermal decomposition technique is widely used to obtain SPIONs with controlled size and morphology, narrow size distribution and crystallinity (Dadfar et al., 2019; Salvador et al., 2019).

This technique requires the use of an iron precursor, usually organometallic compounds such as acetylacetonates in the presence of surfactants, commonly oleylamine and oleic acid. It can be performed in a solvent or solvent-free environment however, the use of stabilizer agents is always required since they bind to the particles nuclei and act as a steric barrier, impeding aggregation and uncontrolled nuclei growth (Bose et al., 2016; Sodipo & Aziz, 2016; Wallyn et al., 2019).

The technique is based on the decomposition of the iron precursor using high temperatures. The process requires the use of two temperatures corresponding to the nucleation and growth steps. A nitrogen atmosphere is also required during the synthesis in order to obtain

SPIONs mainly composed by magnetite, preventing its oxidation to maghemite (Wallyn et al., 2019).

The SPIONs obtained via this method are usually hydrophobic due to the use of hydrophobic surfactants. This way, for biomedical applications an additional step should be performed to modify the SPIONs surface to a hydrophilic one. For that purpose, polymers are widely used (Salvador et al., 2019).

### 3.1.3. Biomedical applications of SPIONs

SPIONs can have many biomedical applications, being the most important ones their ability for drug delivery, magnetic hyperthermia and contrast agents in MRI (Miguel et al., 2020).

MRI is one of the most important imaging methods for diagnosis. Contrast agents are usually used in MRI to enhance the image obtained. Most of them are composed by gadolinium complexes; however these show some important concerns such as short blood circulation times and toxicity. To overcome these problems, the search for new contrast agents increased and the SPIONs have shown to be a good candidate. Moreover, there are already several formulations that are approved by FDA for human use, such as Lumiren®, Feridex IV® and Combidex® (Stephen et al., 2011; Yoon et al., 2012).

SPIONs can be delivered to the human body in a non-invasive manner, which makes them an ideal candidate for drug delivery (Deatsch & Evans, 2014). They are able to drag drug molecules and drive them to the target site with an external magnetic field due to their magnetic properties (Wahajuddin & Arora, 2012).

The magnetic properties of SPIONs also make them useful for magnetic hyperthermia applications. Hyperthermia is a procedure that consists of heating a target tissue above the physiological temperature (Deatsch & Evans, 2014). This approach is mainly used for cancer treatment since this heating (temperatures above 42ºC) can cause cancer cell death or make them more sensitive to other therapeutical approaches (Li et al., 2017; Salunkhe et al., 2014). Regarding AD, recent studies have shown the potential of hyperthermia to break Aβ *in vitro* (Dyne et al., 2021).

## 3.2. Lipid-Polymer hybrid nanoparticles

Lipid-based nanocarriers and polymeric nanoparticles are the most investigated and commonly used types of nanocarriers due to their biocompatible and biodegradable properties.

Recently, polymeric nanoparticles (PNPs) have been widely studied and have even entered pre-clinical development. They are characterized by their small dimensions with a high capacity to encapsulate poorly water-soluble drugs. These nanoparticles allow a controlled drug release at the target site over a period of time (Li et al., 2017). The drug release depends on the polymer chosen and its degradation (Dave et al., 2019). They also constitute a shell that protects the drug from enzymatic and hydrolytic degradation (Tsou et al., 2017).

PNPs surface can constitute a barrier to its use because of its hydrophobicity. This characteristic makes the nanoparticle recognizable as a foreign agent, which can result in a rapid elimination from systemic circulation (Bose et al., 2016). However, PNPs surface can be easily functionalized with lipids that confer the nanoparticle biomimetic advantages or can also be functionalized using targeting ligands which allows personalized therapies for targeted drug delivery (Zhang et al., 2008). Despite the biocompatibility associated with PNPs it is not as high as the lipid-based nanocarriers biocompatibility (Liu et al., 2010).

The synthesis process of these nanoparticles is simple and can be easily scalable (Zhang et al., 2008). However, besides the advantages associated with PNPs, there are some drawbacks that cannot be circumvented, such as the need to use toxic organic solvents in the synthesis process (Persano et al., 2021).

Liposomes are spherical vesicles with a lipid bilayer structure that have been widely used since their discovery (Dave et al., 2019). Similar to PNPs, liposomes are a type of vehicle able to deliver both hydrophobic and hydrophilic compounds (Cheow & Hadinoto, 2011; Dave et al., 2019). The ability to deliver both types of compounds is acquired due to the phospholipidic structure that constitutes the nanoparticle, being composed of a hydrophilic head and hydrophobic tails (Liu et al., 2010). However, liposomes are less effective when encapsulating hydrophobic compounds compared to PNPs (Dave et al., 2019).

Liposomes have a low production cost; however they also have some drawbacks such as a reduced stability and structural integrity, especially when compared to PNPs, and it also promotes a fast drug release instead of a controlled drug release during a certain period (Cheow & Hadinoto, 2011; Persano et al., 2021).

Several liposomal formulations are already FDA-approved for clinical use. The first one approved was AmBisome® (amphotericin B) in 1990, followed by Doxil® in 1995 and by Myocet® in 1999, being the two last ones composed of doxorubicin in liposomes. Other formulations already approved are DepoCyt® (cytarabine), DepoDur® (morphine), Visudyne® (verteporfin) and DaunoXome® (daunorubicin) (Y. Liu et al., 2010; Mukherjee et al., 2019; Shah & Misra, 2004; L. Zhang et al., 2008)

Lipid-polymer hybrid nanoparticles (LPHNPs) constitute a novel drug delivery system approach designed to integrate the advantages of both liposomes and polymeric nanoparticles

in a single nanosystem. They are composed of two layers, the inner polymeric core that can encapsulate hydrophobic drugs and the lipid layer that surrounds the polymeric core. This structure can be observed in Figure 3.4– C. Additionally, an outer PEG layer can also be added to increase the stability of the nanosystem, prolong their circulation half-life and protect against immune recognition (Bose et al., 2017; Dave et al., 2019; Mukherjee et al., 2019).

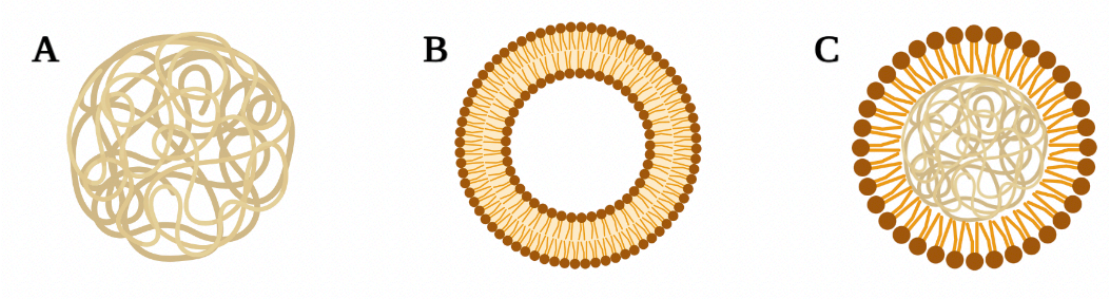


**Figure 3.4** Representation of different types of nanoparticles. A - Polymeric nanoparticle; B - Liposome; C - Lipid-Polymer hybrid nanoparticle.

This type of nanosystem combines the biomimetic nature and biocompatibility of the liposomes with the controlled drug release profile and the ease of being functionalized of the PNPs (Persano et al., 2021). It also allows overcoming disadvantages present in liposomes and PNPs such as structural disintegration, limited circulation time, and content leakage (Mukherjee et al., 2019). Due to their unique characteristics, LPHNPs are receiving much attention in clinical trials (Bose et al., 2017).

To produce LPHNPs, many different polymer-lipid combinations can be used that reinforces the versatility associated with this type of nanoparticles. One of the most used lipid-polymer combinations is PLGA-lecithin.

### 3.2.1. Polylactic-co-glycolic acid (PLGA)

Polymers of natural and synthetic origin have been used to synthesize PNPs. One of the most used polymers for fabricating PNPs is the PLGA that is approved by Food and Drug Administration (FDA) for human use (Vergoni et al., 2009).

PLGA is a copolymer constituted by monomers of lactic acid and glycolic acid (Figure 3.5) that is widely used mainly because of its biocompatibility and biodegradability (Ghitman et al., 2020).

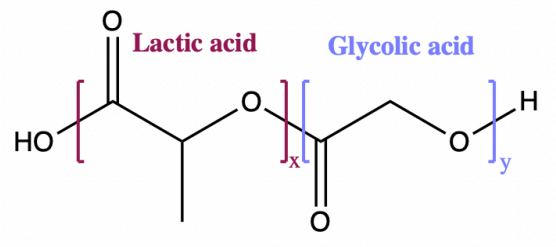


**Figure 3.5** Structure of PLGA

At the time of degradation, the copolymer suffers hydrolysis and degrades into two different metabolites, lactic and glycolic acid. These metabolites are natural and are easily eliminated from the body as carbon dioxide and water via the Krebs cycle, thus presenting no relevant toxicity (Amo et al., 2021; Feltrin et al., 2022).

The degradation time of this polymer will depend on the copolymer ratio. For example, the lactic acid is more hydrophobic; so, in copolymers with a higher ratio of lactic acid the degradation will be slower because the polymer will have less tendency to absorb water (Miladi et al., 2014).

Another important feature related to the copolymer ratio, which is intrinsically linked to the degradation time, is the drug release. The drug release from PLGA nanoparticles is expected to be sustained and controlled; however, a copolymer ratio that leads to a faster degradation time will promote a faster and less controlled release of the drug from the nanoparticle. The most used ratio is 50:50 because it promotes a medium/fast drug release (Amo et al., 2021).

### 3.2.2. Lecithin

Lecithin/phosphatidylcholine is a phospholipid widely used in the food and pharmaceutical industries mainly as an emulsifier and nutrition enhancer (Jardim et al., 2020). It can be found in nature in some vegetables such as soybeans and in animal sources such as egg yolk and milk. The most advantageous type of lecithin to use is soybean lecithin that contains less polyunsaturated fatty acids when compared to lecithin from animal sources, which is responsible for more stability and it is also more economical (Le et al., 2019).

Cell membranes are composed of phospholipid bilayers and lecithin constitutes one of the phospholipids widely present in those structures, this way it can be said that lecithin is highly biocompatible (Elmeshad & Tadros, 2011).

The use of lecithin to coat nanoparticles has shown to be advantageous since it increases the biocompatibility of the nanosystem, increases its stability and the circulation half-life and decreases its immunogenicity (Gong & Winnik, 2012). Lecithin can also act as a surfactant in

nanoparticles production; however it cannot act alone because it is not enough to stabilize the system, the electrostatic repulsion between the particles produced using lecithin as the only surfactant is not strong enough to avoid aggregation (Mandal et al., 2013).

### 3.2.3. Synthesis of LPHNPs

#### 3.2.3.1. Nanoprecipitation method

Nanoprecipitation is a single-step method and the most used technique to produce LPHNPs, mainly due to its simplicity and reproducibility (Persano et al., 2021). This technique requires using a water-miscible organic solvent, usually acetone, ethanol, or acetonitrile, to dissolve either the polymer and the drug, and an aqueous phase (non-solvent) containing the surfactant and the lipids in solution (Bose et al., 2016). The aqueous phase should be previously heated to obtain a well-dispersed lipid solution (Persano et al., 2021). One limitation of this technique is that it only allows the encapsulation of hydrophobic drugs (Miladi et al., 2014).

The technique consists of adding dropwise the organic phase to the non-solvent under constant stirring. This will promote the precipitation of the polymer into nanoparticles and the self-assembly of lipid molecules on the nanoparticles' surface through hydrophobic interactions during solvent evaporation. It occurs to reduce the free energy of the system. (Bose et al., 2016; Cheow & Hadinoto, 2011; Mandal et al., 2013) The hydrophobic interactions allow the formation of the lipid monolayer that consists of the hydrophobic tails directed toward the polymeric core and the hydrophilic heads facing the external aqueous surrounding (Bose et al., 2016).

This technique goes through three different steps from its inception until reaching the final nanoparticles' suspension. The steps are nucleation, growth, and coagulation/aggregation and they are represented in Figure 3.6 (Martínez Rivas et al., 2017).

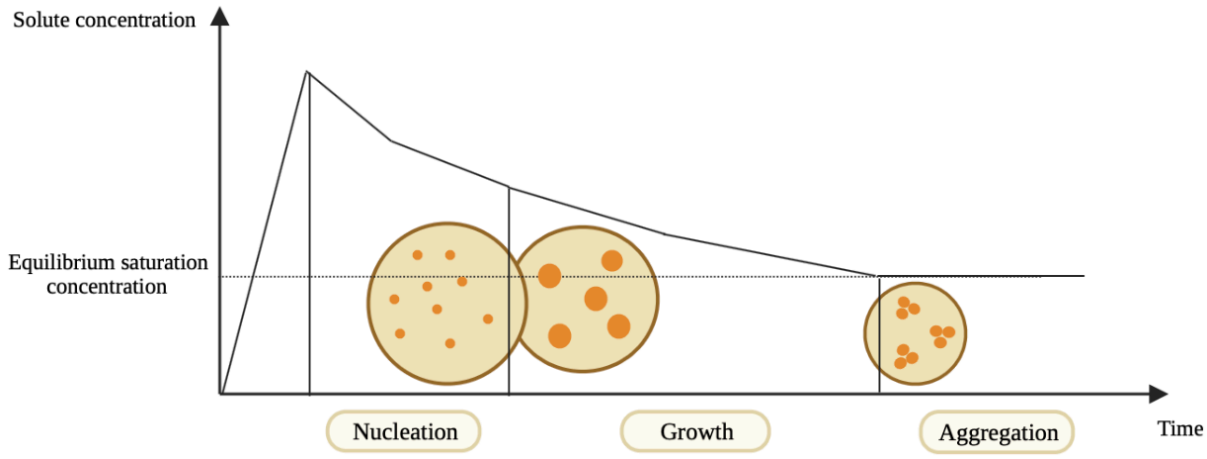


**Figure 3.6** Schematic representation of the nanoprecipitation steps over time. Adapted from (Martínez Rivas et al., 2017)

When the organic phase is added to the non-solvent, its potency to dissolve the solute (polymer) decreases, leading to the supersaturation of the polymer (Martínez Rivas et al., 2017; Pustulka et al., 2013). This supersaturation acts as the driving force for the nanoparticle's formation. With the supersaturation, the system is thermodynamically unstable, and at this point, the nucleation step starts to occur to increase the thermodynamic stability. This stability is reached when the solution is no longer saturated. At this point the solute concentration reaches the equilibrium saturation concentration (Yan et al., 2021).

The last step of this technique is aggregation, which consists of adhesion between particles when the attractive interactions are stronger than repulsive ones. It can be avoided by adding surfactants that will produce repulsive interactions becoming stronger than the attractive ones (Martínez Rivas et al., 2017).

### 3.2.3.2. Single emulsion-solvent evaporation method

The single emulsion-solvent evaporation method is widely used to develop particulate nanocarriers, especially for encapsulating hydrophobic drugs (Miladi et al., 2014). Similar to the nanoprecipitation technique, this technique also requires the dissolution of the polymer, lipid, and all the components to encapsulate in an organic solvent. However, in this case, the organic solvent must be water-immiscible (Dave et al., 2019). The most used organic solvents in this technique are dichloromethane (DCM), chloroform, or ethyl acetate (Jenjob et al., 2019; Miladi et al., 2014).

The formulation of an oil-in-water (o/w) emulsion is required in this method. The emulsification has a huge impact on the nanoparticle's size obtained because it is responsible for the droplet formation that will lead to the obtained nanoparticles (Deshmukh et al., 2016).

To obtain the emulsion, the organic phase is added to an aqueous phase containing a surfactant and dispersed using ultrasonication. Once the emulsion is obtained, the evaporation of the organic solvent is required. It can be performed either by moderate stirring at room temperature or under reduced pressure (Nava-Arzaluz et al., 2012). The evaporation leads to the precipitation of the polymer as nanoparticles.

Some factors may affect the obtained nanoparticles with this technique, such as the polymer concentration, the surfactant used, and its concentration (Nava-Arzaluz et al., 2012).

## 3.3. Functionalization of the nanoparticles via EDC/NHS reaction

The most widely used strategy to functionalize nanoparticle's surface is (N-ethyl-N′-(3-(dimethylamino)propyl)carbodiimide/N-hydroxysuccinimide) (EDC/NHS) chemistry (Peña-Bahamonde et al., 2018; Raghav & Srivastava, 2016).

The reaction involves the use of EDC, a water-soluble cross-linker agent, and NHS (or sulfo-NHS) that acts as a nucleophile (Barbosa et al., 2015; Peña-Bahamonde et al., 2018). This method allows the formation of amide bonds between the carboxyl and amine groups (Bartczak & Kanaras, 2011; Song et al., 2021) The schematic representation of the EDC/NHS coupling can be seen in Figure 3.7.

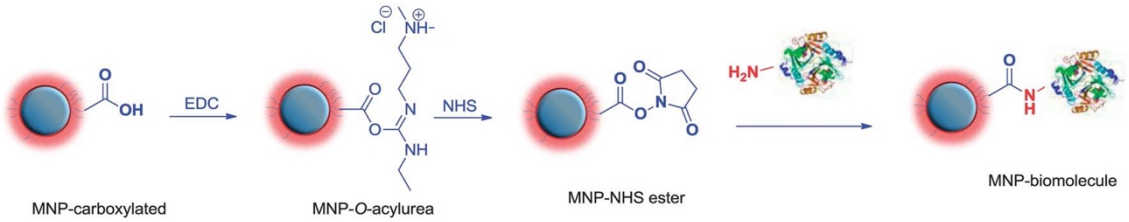


**Figure 3.7** EDC/NHS coupling reaction between nanoparticles and biomolecules. Retrieved from (Turcheniuk et al., 2013)

Briefly, the first step is the activation of the carboxyl groups by EDC which leads to the formation of the intermediate O-acylurea. Then, the NHS or sulfo-NHS reacts with the intermediate O-acylurea to promote its stabilization. This forms the NHS ester intermediate that is still reactive but more stable than the O-acylurea (Barbosa et al., 2015; Song et al., 2021). Then, when in contact with a protein with an amine group, a covalent bond is formed (Jazayeri et al., 2016).

# Chapter 2

# Aims of the study

AD is the leading cause of dementia in the world. It is estimated that approximately 44 million people worldwide lives with AD or a related form of dementia.

Nowadays, the lack of an efficient therapeutic approach to treat AD is a concern due to the prevalence of the pathology in the society. For that reason, is important to find an efficient approach that would treat the disorder, ideally in a local manner. A recent approach to treat AD and to delivery, in general, drug to the CNS is using nanotechnology. The nanotechnological approaches can include the encapsulation of a drug that is not able to freely cross the BBB in nanoparticles with a small size enough to cross the BBB and, that way, deliver the drug in the CNS.

For that reason, this master thesis has the main goal of developing a nanosystem composed by SPIONs (can act as MRI contrast agents) and curcumin encapsulated in lipid-polymer hybrid nanoparticles functionalized with a CPP, responsible to increase the permeability of the nanosystem through the BBB. The structure of the proposed nanosystem is schematized in Figure 3.8.

The main aims of the work are:

1. Synthesize superparamagnetic iron oxide nanoparticles by thermal decomposition technique;
2. Produce lipid-polymer hybrid nanoparticles and encapsulate in them SPIONs and curcumin;
3. Functionalize the nanoparticles with a CPP to provide a high permeability of the nanosystem through the barrier;
4. Nanoparticles cytotoxicity assessment in a human brain endothelial cell line;
5. Evaluation of nanoparticle's uptake by a human brain endothelial cell line.

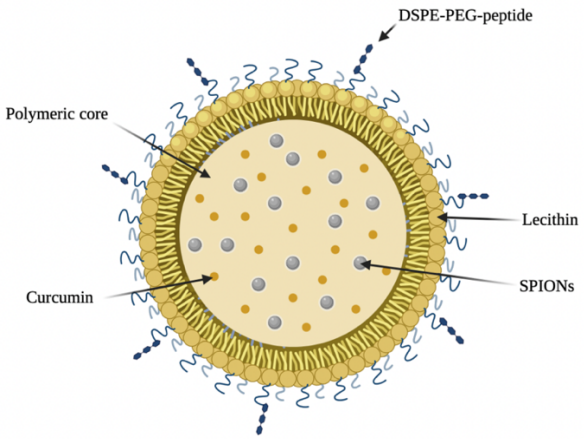


**Figure 3.8** Schematic representation of the proposed nanosystem

# Chapter 3

# Materials and Methods

## 4. Nanosystem

### 4.1. Materials

Tris(acetylacetonate) iron (III) ($Fe(acac)_3$) and 1,10-phenantroline monohydrate were acquired from Alfa Aesar (Haverhill, Massachusetts, USA). From Sigma-Aldrich (St Louis, MO, USA) were purchased oleylamine, hydroxylamine hydrochloride, Pluronic F127, sodium cholate, N-ethyl-N′-(3-(dimethylamino)propyl)carbodiimide (EDC) and N-Hydroxysuccinimide (NHS). The Polylactic-co-glycolic acid with a 50:50 monomer (PLGA (50:50)) was purchased from Corbion (Amsterdam, Netherlands). Ammonium acetate was purchased from Panreac, soya lecithin (Lipoid S100) from Lipoid (Ludwigshafen, Germany) and 1,2-distearoyl-sn-glycero-3-phosphoethanolamine-N-[carboxy(polyethylene glycol-2000] from Avanti Polar Lipids, Inc.

### 4.2. Synthesis of SPIONs

To synthesize SPIONs a thermal decomposition method was used. For that, a solution with 2 mmol of $Fe(acac)_3$ and 20 mL of oleylamine was made. This solution was magnetically stirred at 500 rpm under a continuous nitrogen flow. The system was closed and refluxing. Then, the solution was heated to 120 ºC for 1 h and then to 300 ºC for 2 h.

After that, 10 mL of ethanol were added to the solution to precipitate the SPIONs. Then, they were collected by centrifugation at 9500 rpm for 10 min. The obtained SPIONs were washed 3 times using an ethanol/hexane mixture (1:2). Finally, they were dispersed in DCM.

### 4.2.1. Spectrophotometric Determination of Iron by UV-Vis

To quantify the SPIONs solution obtained by thermal decomposition, a spectrophotometric method can be used. This method determine the iron content using the 1,10-phenantroline colorimetric method (Soares et al., 2014).

Briefly, 40 µL of a diluted SPIONs suspension were added to an empty eppendorf followed by the addition of 20 µL of HCl 37% (v/v) that react for 1 h to dissolve SPIONs in ferrous and ferric chloride. After that, 100 µL of a hydroxylamine hydrochloride 100 $mg.mL^{-1}$ and 500 µL of 1,10-phenantroline monohydrate solution 3 $mg.mL^{-1}$ were added to reduce all Fe (III) into Fe (II). Finally, to dilute the samples 1140 µL of ammonium acetate 500 mM pH 4 buffer were added. All samples were made in triplicate.

The absorbances were obtained by measuring the absorbances at 510 nm using a UV-Vis spectrophotometer (T90+ UV/VIS Spectrometer PG Instruments Ltd).

To obtain the nanoparticles concentration in $mg.mL^{-1}$ the formula used was [Fe]=0.7×[NPs].

## 4.3. Lipid-polymer hybrid nanoparticles (LPHNPs)

### 4.3.1. Nanoprecipitation

The nanoprecipitation method can be used to produce both LPHNPs and polymeric nanoparticles.

For that, 20 mg of PLGA with a 50:50 monomer was dissolved in 1 mL of acetone, acetonitrile, dimethylformamide (DMF) or tetrahydrofuran (THF). Then, it was added dropwise to 20 mL of Pluronic F127 solution 0.3% 0.5%, 1% or 2% (w/v) under magnetic stirring at 300 rpm and the obtained colloid was kept in agitation for 2-3 h to evaporate the solvent.

To collect the nanoparticles produced, they were centrifuged for 20 min at 10000 rpm at 4ºC and then they were washed 3 times with water by centrifugation with the same specs referred before. Finally, the obtained nanoparticles were resuspended in water.

### 4.3.2. Single emulsion/Solvent evaporation

The single emulsion/solvent evaporation technique was the preferred technique to produce LPHNPs.

Briefly, 10 mg of PLGA, 0.5 mg of SPIONs and 2 mg of curcumin were dissolved in 800 µL of DCM and 200 µL of a stock solution of soy lecithin with a concentration of 360 mg/mL

was also added. The resultant solution was then added dropwise to a water phase composed of 5 mL of sodium cholate 1% (w/v). Then, the emulsion was produced during a 30 second period of ultrasonication using UP400St Powerful ultrasonicator (Hielscher Ultrasonics), and then stirred for 2 h to evaporate the solvent.

The suspension of nanoparticles obtained was split into 1.5 mL eppendorfs and collected by centrifugation at 30000 xgs for 15 minutes and resuspended in 1 mL of water.

#### 4.3.2.1. Determination of curcumin using fluorescence

To quantify the amount of curcumin non-encapsulated, the obtained nanoparticles were first collected by centrifugation, and the supernatant was analyzed using fluorescence.

For that, a calibration curve was done to quantify the mass of curcumin in the supernatant. This mass corresponds to the curcumin that was added to the formulation and wasn't encapsulated in the nanoparticles.

Briefly, in a 96-well microplate add 20 µL of the supernatant in three different wells. The fluorescence values were obtained by measuring the emission fluorescence at 520 nm using the fluorimeter FLUOstar Omega (BMG Labtech).

## 4.4. Functionalization of LPHNPs with a CPP via EDC/NHS

The EDC/NHS reaction is widely used to functionalized nanoparticles. In this case, the functionalization is performed not directly in the nanoparticle's surface but to a phospholipid that will be after adsorbed into the nanoparticle surface.

First, in a 1.5 mL Eppendorf add 200 µL of DSPE-PEG-COOH solution 10 mg/mL. Then, add 400 µL of EDC solution 0.5 M and 400 µL of NHS solution 0.5 M and keep the reaction at room temperature for 3 h under gentle stirring. After that, remove the EDC and NHS excess with a dialysis membrane MWCO 1kDa in HEPES buffer 7.4 Add 100 µL of CPP solution 2 mg/mL in HEPES to the previous dialyzed solution and keep the conjugation at room temperature for 2 h, followed by overnight incubation at 4ºC in a refrigerator.

On the next day, to remove the uncouple CPP a dialysis membrane 3.5 kDa was used and the coupling efficiency was measured using UV.

The obtained DSPE-PEG-CPP is then added to a previously produced suspension of nanoparticles to be adsorbed on the surface. The reaction was kept for 2 h and, in the end, to remove the DSPE-PEG-CPP that did not adsorb, a dialysis membrane MWCO 3.5 kDa was used. In the end, the efficacy of the adsorption was also assessed using UV by measuring the emission fluorescence at 360 nm.

## 4.5. Characterization of nanoparticles

Produced nanoparticles were characterized using different techniques. These types of analysis give information about the nanoparticle's size, hydrodynamic diameter, morphology, and composition.

### 4.5.1. X-Ray Diffraction (XRD)

The XRD is an analytical technique used for characterization of materials. The technique allows the study of the crystalline structure of the samples by beaming them with x-rays. The XRD patterns of the samples (they act like fingerprints of the materials) are compared to the standard reference patterns from the Joint Committee on Powder Diffraction Standards (JCPDS) library to identify the crystalline form. Besides that, further analysis of the obtained XRD pattern can be done to obtain the average crystallite size (Khan et al., 2020; Kim et al., 2013; Titus et al., 2019).

Samples analyzed through XRD were freeze-dried. The analysis was performed in a X'Pert PRO MDP (PANalytical) X-ray diffractometer, with a $2\theta$ from 15º to 80º using Cu-Ka radiation (k = 1.54060 Å) with a step size of 0.033.

### 4.5.2. Fourier Transform Infrared (FTIR) Spectroscopy

FTIR spectroscopy is a highly used technique for characterizing nanoparticles regarding their chemical composition. The technique allows the identification of the functional groups present in a sample, by beaming the sample with infrared light, and then measuring the intensity of the passing radiation at each wavenumber (Faghihzadeh et al., 2016; López-Lorente & Mizaikoff, 2016) The absorbed radiation is then converted to vibrational or rotational energy, allowing the identification of chemical groups (Titus et al., 2019).

Samples were freeze-dried before the analysis that was performed using the Spectrum Two™ FT-IR Spectrometer (PerkinElmer) with Attenuated Total Reflectance (ATR). The Image J software was used to analyze the images obtained in order to obtain a size distribution graphic.

### 4.5.3. Transmission Electron Microscopy (TEM)

TEM is a type of microscopy that allows the visualization of atomic-scale structures. In nanotechnology, TEM is widely used for morphological analysis and to determine the core size of nanoparticles (Lin et al., 2021).

Samples were prepared by diluting the original stocks. The TEM images were acquired using a Hitachi H-8100 II with thermionic emission LaB6 from Instituto Superior Técnico.

### 4.5.4. Superconducting Quantum Interference Device (SQUID)

The magnetic characterization of nanoparticles was performed using SQUID. The magnetization of the nanoparticles can be measured as a function of temperature and/or field.

For the nanoparticle's analysis, the samples were freeze-dried. Then, the measurement was performed using the SQUID magnetometer S700X (Cryogenic Ltd) from Instituto Superior Técnico. The magnetization curves were obtained for temperatures of 10 and 305 K and for fields up to 5 T.

### 4.5.5. Dynamic light scattering (DLS)

The DLS characterization gives information regarding the size, polydispersity index (PI) and zeta potential of the nanoparticles in suspension.

The technique is based on measuring the intensity fluctuations of the light scattered by nanoparticles over time, after illuminating the suspension with a monochromatic laser beam, obtaining this way the diffusion coefficients (Murdock et al., 2008; Zheng et al., 2016).

The random movement that nanoparticles can acquire due to their Brownian motion (movement to which the nanoparticles are subjected due to the random collisions that occur with other molecules present in the nanoparticle's suspension) results in different values of diffusion coefficient since smaller nanoparticles move faster and diffuse faster than larger nanoparticles (Ramos, 2017; Zheng et al., 2016). To calculate the nanoparticle's hydrodynamic radius, the Stokes-Einstein equation **(Equation 4.1)** can be used:

$$D = \frac{k_b T}{6\pi\, \eta R_h} \qquad \textbf{Equation 4.1}$$

Where D is the diffusion coefficient, $k_b$ is the Boltzman constant, T is the absolute temperature in Kelvin, $\eta$ is the viscosity of the dispersing medium and $R_h$ is the hydrodynamic radius of the nanoparticle (Carvalho et al., 2018; Ramos, 2017).

The DLS characterization was performed on a Malvern Instruments Zetasizer 1000HSA equipment.

## 4.6. Cell Culture

### 4.6.1. Materials

Human cerebral microvascular endothelial cells (HBEC- 5i, ATCCR CRL-3245) were purchased from American Type Culture Collection (ATCC, United States). From Gibco/Thermo Fisher were purchased gelatin, DMEM:F12 medium, penicillin/streptomycin antibiotic solution , FBS and trypsin-EDTA. Endothelial growth supplement (ECGS) was acquired from Sigma-Aldrich (Spain) and the RealTime-Glo™ MT Cell Viability Assay from Promega (USA).

### 4.6.2. Culture of human cerebral microvascular endothelial cells

HBEC-5i cells were cultured as a monolayer on 0.1% gelatin solution coated T-flasks in DMEM:F12 medium supplemented with 10% FBS, 1% penicillin/streptomycin antibiotic solution, and 40 mg/mL endothelial growth supplement (ECGS) according to the manufacturer's instructions. Cells were grown in a humidified atmosphere of 5% $CO_2$ at 37ºC (MCO-18AIC (UV), Sanyo, Japan) with the medium changed every other day.

### 4.6.3. Cell viability measurements

To analyze the cytotoxicity of the produced nanoparticles against HBEC-5i cells the RealTime-Glo™ MT Cell Viability Assaywas used according to the manufacturer's protocol. This assay determines the number of viable cells in culture by measuring the reducing potential of cells and thus metabolism.

The assay consists in adding NanoLuc® luciferase and a cell-permeant prosubstrate, to cells in culture. Then, the viable cells reduce the proprietary prosubstrate to generate a substrate for NanoLuc® luciferase. This substrate diffuses from cells into the surrounding culture medium, where it is rapidly used by the NanoLuc® Enzyme to produce a luminescent signal.

Briefly, HBEC-5i cells were carefully harvested from T-flasks with trypsin-EDTA and seeded 20,000 cells.mL$^{-1}$ (100 µL per well) in 0.1% gelatin solution coated 96-well white flat bottom plates (Corning, United States) and incubated for 24 h. Then, the medium was removed

and 60 µL of fresh DMEM:F12 medium containing a known concentration of nanoparticles (ranging from 0.10 to 100 µg.mL$^{-1}$) were added to each well in triplicates. After that, the RealTime-Glo™ reagent was prepared by diluting the MT Cell Viability Substrate and NanoLuc® Enzyme in DMEM:F12 medium to a 2X concentration for each reagent and added in an equal volume of diluted nanoparticles (60 µL) to the cells. Luminescence was then measured on a Varioskan LUX Multimode Microplate Reader (Thermo Fisher Scientific, United States) which have an integrated gas control and incubator system that allowed cells incubation in a humidified atmosphere of 5% CO2 at 37ºC for 48 h.

Cells in the medium and cells in 1% Triton X-100 containing medium were used as positive and negative controls, respectively. To obtain the cell viability results the following equation (**Equation 4.2**) must be used:

$$\text{Cell Viability (\%)} = \frac{RFU_{NPs} - RFU_{NC}}{RFU_{PC} - RFU_{NC}} \times 100 \qquad \textbf{Equation 4.2}$$

Where $RFU_{NPs}$ is the luminescence obtained for the nanoparticles-treated cells, $RFU_{NC}$ the luminescence of negative controls and $RFU_{PC}$ the luminescence value of positive controls.

### 4.6.4. Flow cytometry

To perform the assay, HBEC-5i cells were seeded 100,000 cells/mL (500 µL per well) in 0.1% gelatin solution coated 24-well flat-bottomed plates for 24 h. Then, the medium was removed, and cells were washed twice with PBS and once with fresh medium. After that, they were incubated for two different time-points (0.5 and 24 h) with nanoparticles, at a final concentration of 25 µg.mL-1 in fresh medium under a humidified atmosphere of 5% $CO_2$ at 37 °C. As a control, the cells were maintained in culture medium.

After incubation, cells were carefully washed twice with 250 µL of medium and once with the same volume of PBS and harvested from each well with 200 µL trypsin-EDTA. Finally, cells were collected and centrifuged at 2,000 rpm, 4°C, for 5 min. After the supernatant was discarded, the cell pellet was washed twice with cold 1× PBS, centrifuged at 2,000 rpm and resuspended in 300 µL of cold 1× PBS. The fluorescence intensity of 10,000 cells was analyzed with a BD LSRFortessa X-20 flow cytometer (BD Biosciences, United States) using laser Alexa Fluor 488. The mean fluorescence of samples was obtained by subtracting the autofluorescence

of cells. All experiments were performed in duplicates. The data were analyzed using FlowJo v10 by MFI determination.

# Chapter 4

# Results and Discussion

## 5. SPIONs obtained by thermal decomposition

### 5.1. Structural Characterization

The XRD analysis allows evaluation of the crystalline structure of the obtained nanoparticles.

In Figure 5.1 it is possible to observe the XRD pattern of the SPIONs coated with oleylamine synthesized through the thermal decomposition method. The graphic shows five characteristic $2\theta$ peaks at 30.1, 35.4, 43.1, 57.1 and 62.6, which correspond to the diffraction plans (220), (311), (400), (511) and (440), respectively (Soares et al., 2015).

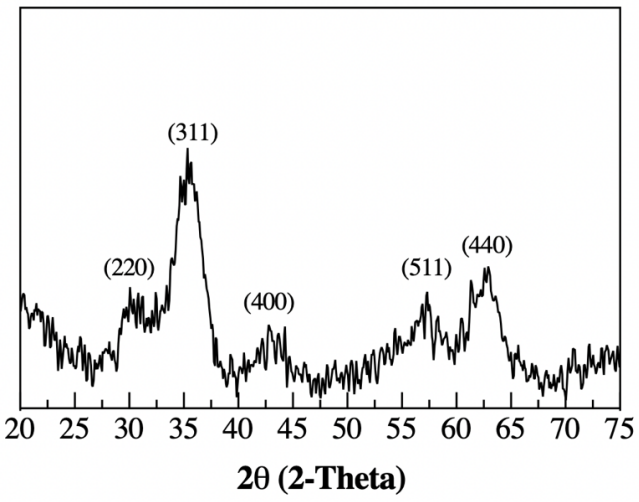


**Figure 5.1** X-ray pattern of iron oxide nanoparticles produced by thermal decomposition.

When comparing the XRD pattern obtained for these SPIONs to the XRD patterns of maghemite (JCPDS 00-039-1346) and magnetite (JCPDS 00-019-0629) powders, it is possible to index the peaks to a crystalline cubic structure.

The obtained XRD pattern shows broad peaks which are consistent with nano-sized crystallites (Matos et al., 2019). To confirm that, the average crystallite size can be calculated using the Scherrer's Equation **(Equation 5.1)**:

$$\tau = \frac{K\lambda}{\beta cos\theta} \qquad \textbf{Equation 5.1}$$

Where $\tau$ is the average crystallite size, K is the grain shape factor (K=0.94), $\lambda$ is the incident x-ray wavelength, $\beta$ denotes the full width at half-maximum of the highest intensity, and $\theta$ is the corresponding diffraction angle (Soares et al., 2014).

The average crystallite size obtained was around 4.3 nm ($2\theta = 35.43$), confirming the nano-sized crystallites. The low value can be explained by the broad peak, leading to higher values of $\beta$, and consequently reducing the value of $\tau$.

## 5.2. Fourier Transform Infrared (FTIR) Spectroscopy

To analyze the chemical composition, SPIONs were characterized by FTIR spectroscopy. The SPIONs produced in this project are coated by oleylamine, that confers to the SPIONs the hydrophobic properties and stability in solution (Xu et al., 2009). That way, in the FTIR spectrum of SPIONs it must be seen not only bands indicating the presence of the iron oxide, but also bands showing the presence of lecithin. The obtained FTIR spectrum of SPIONs is shown in Figure 5.2.

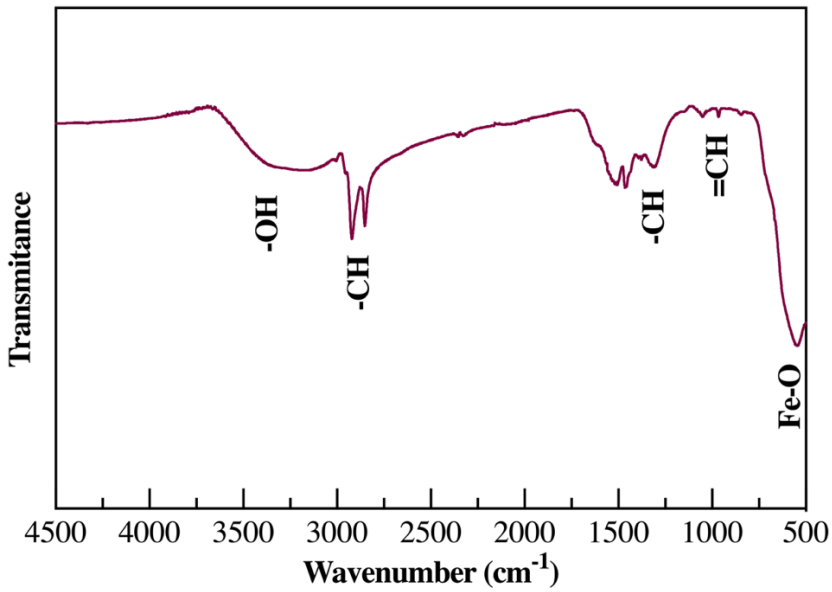


**Figure 5.2** FTIR spectrum of SPIONs produced by thermal decomposition method

From Figure 5.2, it is possible to identify the presence of SPIONs through the band at 543 $cm^{-1}$ derived from Fe-O stretching vibration mode and through the broad band around 3500 $cm^{-1}$ related to the -OH stretching vibration mode (Gaspar et al., 2019; Soares et al., 2014).

Oleylamine structure can be seen in Figure 5.3. Due to its structure, most peaks shown in the FTIR spectrum are related to this compound.

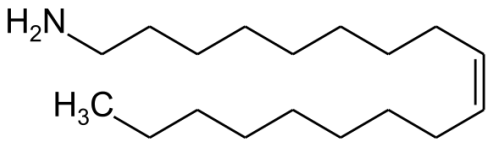


**Figure 5.3** Oleylamine chemical structure

Oleylamine can be identified in the spectrum through different bands, such as the ones at 2851 $cm^{-1}$ and 2920 $cm^{-1}$ due to symmetric and asymmetric stretching vibrations of $CH_2$ groups (Kurtan, Erdemi, et al., 2016; Perez De Berti et al., 2013). Oleylamine also origins the bands seen at 1050 $cm^{-1}$ and 965 $cm^{-1}$ that identify the =CH bending and the bands at 1311-1505 $cm^{-1}$ that are related to the long hydrocarbon chain of oleylamine (Gaspar et al., 2019; Kurtan, Erdemi, et al., 2016).

With this, it is possible to affirm that SPIONs coated with oleylamine were successfully synthesized. Moreover, the absence of characteristic peaks of $NH_2$ group in FTIR spectra

indicates that oleylamine links to SPIONs through the amine group (Kurtan, Güngüneş, et al., 2016; Soares et al., 2014).

## 5.3. Morphological Characterization

The morphological characterization of SPIONs was assessed by using transmission electron microscopy (TEM). The obtained TEM images of SPIONs can be seen in Figure 5.4. Also, in Figure 5.4 it is possible to observe the size distribution graphic. The diameters were assessed using the Image J software and counting 200 SPIONs.

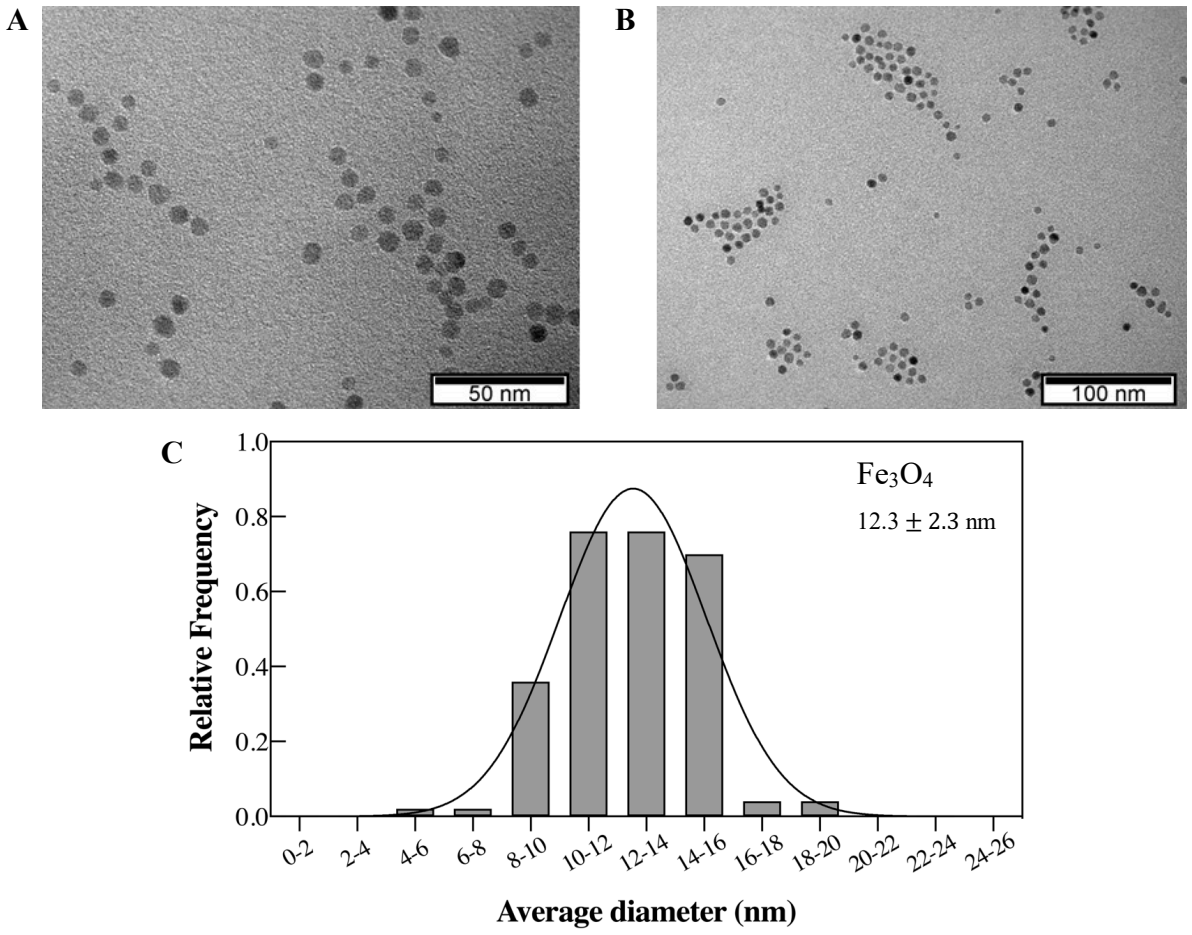


**Figure 5.4** TEM images (A and B) with different scales and the respective size distribution graphic (C) of SPIONs

From Figure 5.4 (A and B) it is possible to affirm that the produced SPIONs do not show significant agglomeration as expected due to the presence of the surfactant oleylamine. It can also be seen that the SPIONs have a spherical morphology ideal for intravenous administration (Schneider et al., 2022).

Regarding the analysis of the diameters, it was possible to assess that the average diameter is 12.3 ± 2.3 nm. This is an important information to remove from this analysis since the size of SPIONs is directly related with their ability to be superparamagnetic. As explained before, for SPIONs to be superparamagnetic their size cannot exceed 15 nm (Dulińska-Litewka et al., 2019). This way, it can be concluded that the produced nanoparticles do not exceed 15 nm indicating, once more, their superparamagnetic behavior and even their ideal characteristics for biomedical applications.

## 5.4. Magnetic Characterization

To assess the magnetic properties of the obtained SPIONs, a superconducting quantum interference device (SQUID) was used. The results were acquired at two different temperatures (10 and 305 K) and the hysteresis loops are shown in Figure 5.5.

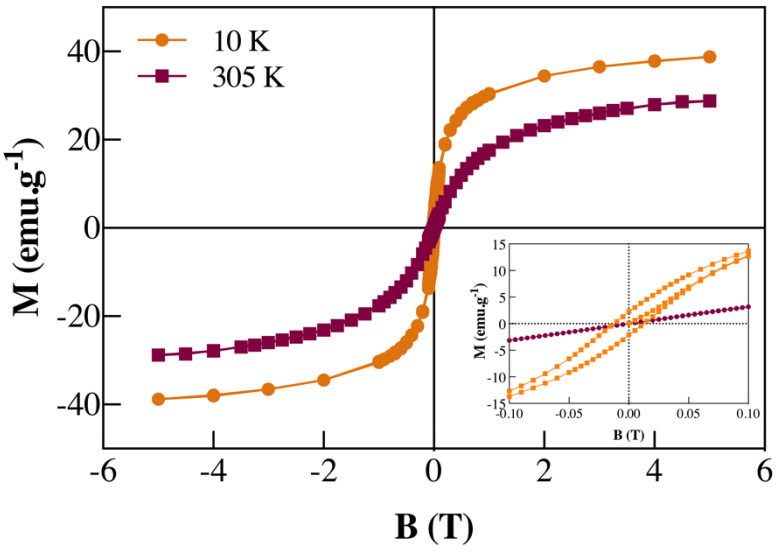


**Figure 5.5** Magnetic characterization of SPIONs produced by thermal decomposition. Graphic of magnetization (M) vs. applied magnetic field (B)

From the graphic, the value of saturation magnetization for each condition can be obtained. For the SPIONs at 10 K the saturation magnetization reaches 38.8 emu.g$^{-1}$ and at 305 K the value decreases to 28.8 emu.g$^{-1}$. These values are low, what can indicate a very small size of the SPIONs, since the smaller the size of the nanoparticle, the smaller the saturation magnetization (Jun et al., 2008).

In Figure 5.2 it is possible to see an enlargement of the center of the graphic, showing the absence of remanence and coercivity at 305 K. However, at 10 K the same cannot be said. In that case, there is a remanence of 2.2 emu.g$^{-1}$ and a coercivity of 100 Oe.

The results obtained confirm the superparamagnetic properties of the obtained SPIONs at 305 K but not at 10 K. This can be explained by the blocking temperature since it represents the temperature below which the nanoparticles cannot acquire a superparamagnetic behavior (Wallyn et al., 2019). In this case, it is possible to conclude that the blocking temperature is a temperature between 10 K and 305 K.

# 6. Polymeric nanoparticles obtained by nanoprecipitation

The nanoprecipitation technique is widely used to produce polymeric nanoparticles. This technique requires the use of a water-miscible organic solvent to solubilize the polymer. The organic solvents mainly used in literature are acetone and acetonitrile.

To test the technique, both acetone and acetonitrile were used to solubilize PLGA and constitute the organic phase. Another organic solvent tested was DMF since it fulfils the requirements for the technique, is water miscible and solubilize the polymer. As aqueous phase, the Pluronic F127 was used and tested at different concentrations to see the effect of it in the nanoparticles size. The results are shown in Figure 6.1.

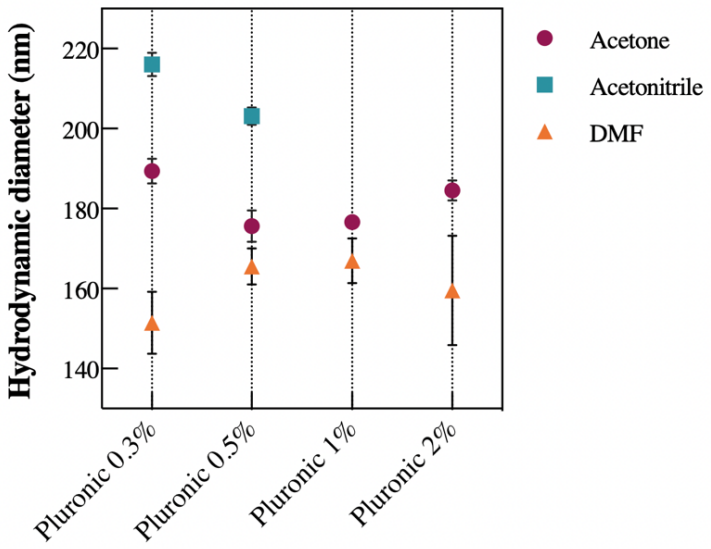


**Figure 6.1** Comparison of hydrodynamic diameters of PLGA nanoparticles obtained by DLS varying the organic solvent and surfactant concentration.

As seen in Figure 6.1, DMF was the organic solvent that promoted the formation of smaller nanoparticles and acetonitrile the one that promoted the formation of larger nanoparticles. According to this information, the preferable organic solvent would be the DMF;

however neither DMF, acetone, or acetonitrile have shown to be able to resuspend SPIONs. The ability of the organic solvent to solubilize both the polymer and SPIONs is a requirement to produce the desired nanosystem since the SPIONs should be encapsulated in the polymeric core.

Another water-miscible organic solvent widely used in nanoprecipitation is THF (Legrand et al., 2007). This organic solvent, contrary to the ones tested before, can resuspend SPIONs (Deok Kong et al., 2013). This way, to promote the encapsulations of SPIONs in the polymeric core the THF should be the organic solvent to use. However, the use of THF has proved to be incompatible with the methodology.

Different approaches were used to optimize the methodology with this solvent; however neither the use of different concentrations of Pluronic F127, the use of vortex after the addition of the organic phase to the aqueous phase, or the use of a mixture of acetone/THF to solubilize the polymer were enough to produce stable nanoparticles.

With this information, the nanoprecipitation technique has shown not to be the best technique to use in this project.

# 7. LPHNPs produced by the single emulsion-solvent evaporation method

## 7.1. Optimization of methodology

The single emulsion-solvent evaporation technique is widely used to produce polymeric nanoparticles and requires the formulation of an oil-in-water (o/w) emulsion.

A previously described protocol was used to start the optimization of the methodology (Lopes et al., 2012). From that, the first surfactant tested is a solution composed of 0.5% (w/v) Tween 20 and 0.6% (w/v) sodium deoxycholate (SD). Several studies were performed by testing different conditions, such as the presence or not of lecithin in the formulation, the time of emulsification and the volume of the surfactant used to create the emulsion (Table 7.1).

**Table 7.1** Conditions tested using 0.5% (w/v) Tween 20 and 0.6% (w/v) SD as surfactant

| | DCM (mL) | Stock solution of lecithin (mL) | Surfactant (mL) | Emulsification (min) | Equipment |
|---|---|---|---|---|---|
| **1** | 0.8 | 0.2 | 10 | 5 | Homogenizer |
| **2** | 1 | 0 | 10 | | |
| **3** | 1 | 0 | 5 | 10 | |
| **4** | 1 | 0 | 10 | | |

From Table 7.1, it is possible to see that between formulations 1 and 2, the difference is the presence of lecithin. In this case, the presence of lecithin did not prove beneficial since after a few hours, formulation 1 showed precipitation of the nanoparticles while formulation 2 did not, indicating this way that the amount of lecithin added to the formulation 1 was excessive.

Formulation 1 was the only one showing precipitation. All others, formulations 2, 3 and 4, have shown colloidal stability and were analyzed using DLS (Figure 7.1).

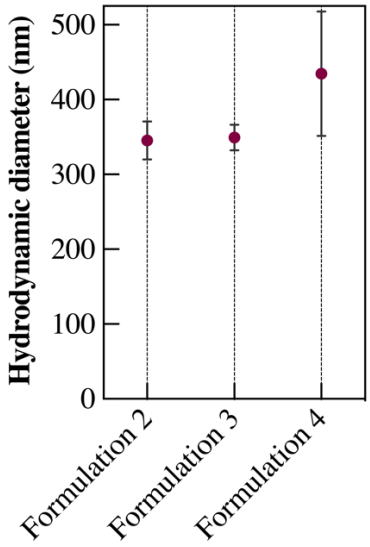


**Figure 7.1** Hydrodynamic diameters obtained from DLS of nanoparticles produced using 0.5% (w/v) Tween 20 and 0.6% (w/v) SD as surfactant

Figure 7.1 shows the hydrodynamic diameters of the nanoparticles produced from formulations 2 to 4. From that, it is possible to compare the influence of the time of emulsification and the volume of surfactant used to produce the emulsion.

To assess the influence of the time of emulsification, formulations 2 and 4 should be compared. From Figure 7.1, it is noted that formulation 4 shows nanoparticles with hydrodynamic diameters much higher than formulation 2. This shows that increasing the emulsification time leads to an increase in the hydrodynamic diameter of the nanoparticles produced.

Then, the influence of the volume of surfactant can be assessed by comparing formulations 3 and 4. In this case, it is also possible to see that increasing the volume of surfactant also leads to an increase in nanoparticles size.

Of the four formulations tested using this surfactant, formulation 3 was the one that produced the nanoparticles with a smaller hydrodynamic diameter ($349.2 \pm 17.2$ nm). However, that size is not small enough so the nanoparticles can be intravenously administered and cross the BBB (Ceña & Játiva, 2018). Since the optimization of the methodology using

0.5% (w/v) Tween 20 and 0.6% (w/v) SD did not show the intended impact on nanoparticle size reduction, another surfactant was tested.

Sodium cholate (SC) is a bile salt negatively charged (anionic) and non-toxic that can act as a surfactant in formulations (Esim et al., 2020). It has a similar structure to SD; however, when comparing them, it is possible to see that SD lacks a 7-hydroxyl group (Ćirin et al., 2012).

To see the effect of changing the surfactant, different parameters were tested when producing nanoparticles with SC as surfactant instead of SD.

**Table 7.2** Conditions tested using 1% (w/v) SC to produce nanoparticles

| | DCM (mL) | Stock solution of lecithin (mL) | Surfactant (mL) | Emulsification (min) | Equipment |
|---|---|---|---|---|---|
| **5** | 1 | 0 | 5 | 5 | Homogenizer |
| **6** | 1 | 0 | 5 | 0.5 | Ultrasonication |

All formulations produced using SC as surfactant have shown colloidal stability. For this case, the conditions tested were the presence of lecithin, the time of emulsification and the equipment used to produce the emulsion (Table 7.2). Also, the obtained hydrodynamic diameters can be seen in Figure 7.2.

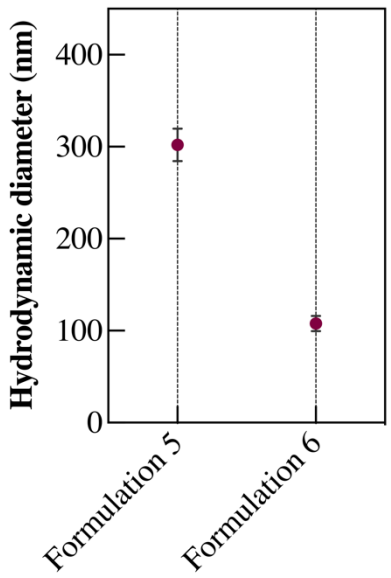


**Figure 7.2** Hydrodynamic diameters obtained from DLS of nanoparticles produced using 1% (w/v) SC

With the previous case, it was assessed that increasing the volume of surfactant and the time of emulsification leads to larger nanoparticles. Since the main goal of using a different surfactant is decreasing the nanoparticle size, the first formulation tested (formulation 5)

combined 5 minutes of emulsification with 5 mL of 1% (w/v) SC. The obtained nanoparticles show a decrease in the hydrodynamic diameter; however, this decrease was not significant enough.

Besides changing the surfactant, another approach to reduce the nanoparticles size can be changing the equipment used to produce the emulsion. It is already reported that the use of a homogenizer leads to larger nanoparticles when compared to ultrasonication (Choi et al., 2014). Ultrasonication produces smaller droplets which, in turn, leads to smaller nanoparticles. For that reason, the use of an ultrasonication probe was tested (formulation 6 and 7).

From Figure 7.2 it is possible to clearly see the influence of the equipment change on the hydrodynamic diameters obtained when comparing formulations 5 and 6. The equipment change leads to a decrease in size from 301.9±17.6 nm (formulation 5) to 107.8 ± 8.3 nm (formulation 6). With this size, the nanoparticles obtained from formulation 6 show the ideal size for the intended application. These show a zeta potential of -42.4 ± 4.9 mV and a PI of 0.067 ± 0.021, indicating that the suspension shows colloidal stability and homogeneous sizes.

Some authors describe the single emulsion-solvent evaporation protocol with an additional step in which they dilute the emulsion in a volume of 0.3% (w/v) SC (Chen et al., 2012; Liu et al., 2013; Ramalho et al., 2018). To assess if there is any significant influence of this dilution on the size of the obtained nanoparticles, studies were performed diluting the emulsion obtained from formulation 6 in 7.5, 15, 20 and 50 mL of 0.3% (w/v) SC and the results are shown in Figure 7.3.

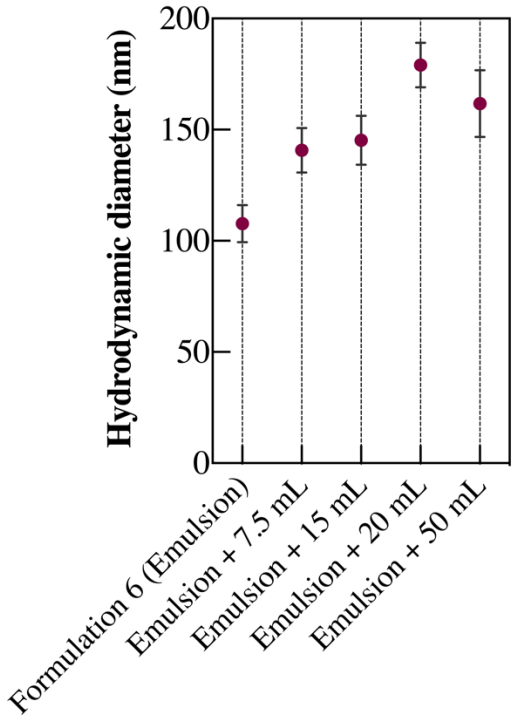


**Figure 7.3** Hydrodynamic diameters obtained from DLS of nanoparticles produced using 1% (w/v) SC to create the emulsion and diluted in different volumes of 0.3% (w/v) SC.

Based on the results presented on Figure 7.3, it is possible to see that diluting the emulsion with any volume of 0.3% (w/v) SC promotes an increase in the nanoparticle's size instead of a decrease. That way, diluting the emulsion does not seem to be a good approach to decrease the nanoparticle's size.

Another optimization performed is related to the purification of nanoparticles. The optimized protocol in the lab to purify the nanoparticles include four centrifugation cycles; the first one to precipitate and collect the nanoparticles, and the rest of them to wash them with water. However, as soon as the SC was used, the nanoparticles started to precipitate after the first centrifugation cycle. For that reason, different number of centrifugation cycles were tested. The nanoparticle's size, PI and zeta potential in each condition tested were obtained (Table 7.3) to see the influence of the number of centrifugation cycles on these parameters.

**Table 7.3** Influence of the number of centrifugation cycles in the size, PI and zeta potential of nanoparticles

| Centrifugation cycles | Size (nm) | PI | Zeta potential (mV) |
|---|---|---|---|
| 0 | 107.7 ± 8.3 | 0.125 ± 0.018 | -54.9 ± 4.7 |
| 1 | 132.5 ± 9.3 | 0.067 ± 0.021 | -44.8 ± 3.9 |
| 4 | 137.9 ± 3.0 | 0.126 ± 0.020 | -37.6 ± 2.5 |

From Table 7.3, it is possible to see that increasing the number of centrifugation cycles leads to an increase in the size of nanoparticles. However, at least one centrifugation cycle is required to remove the SC excess.

It can also be seen that between the nanoparticles that were subjected to one and four centrifugation cycles the PI was highly affected. In this case, from one centrifugation cycle to four the PI value doubled, indicating that after 1 centrifugation cycle, the next ones will lead to nanoparticle's aggregation (Rampino et al., 2013).With this, it is possible to conclude that the best way to purify the produced nanoparticles is using one centrifugation cycle.

Based on all results obtained before, formulation 6 should be taken as the base formulation from this point on. However, with this, the nanoparticles produced are polymeric and not hybrid. So, to obtain the hybrid nanoparticles (composed by the PLGA core and the lecithin layer), lecithin should be added to the formulation to create the lipid shell around the polymeric core.

The same amount of lecithin (0.2 mL of stock solution) tested before, was tested again in the optimized formulation. The hybrid nanoparticles obtained show an average particle size of 108.4 $\pm$ 20.1 nm and a polydispersity index of 0.140$\pm$0.013. These results are slightly higher

than the ones obtained for the polymeric nanoparticles; however they are still good for the intended application.

To confirm the presence of lecithin in the nanoparticles, the zeta potential should be assessed. For the polymeric nanoparticles, the zeta potential obtained was -42.4±4.9 mV and for the hybrid nanoparticles was -24.1±3.9 mV. This increase in zeta size values from polymeric to hybrid nanoparticles indicates the presence of the lecithin lipid layer.

Then, to obtain the proposed nanosystem, it is necessary to encapsulate the previously synthesized SPIONs. For that, two different amounts of SPIONs were added to the base formulation. The results are shown in Table 7.4.

**Table 7.4** Results obtained from DLS of LPHNPs encapsulating different amounts of SPIONs

| | **Size (nm)** | **PI** | **Zeta potential (mV)** |
|---|---|---|---|
| 0.5 mg SPIONs | 91.6 ± 1.6 | 0.157 ± 0.017 | -23.9 ± 4.6 |
| 1 mg SPIONs | 120.6 ± 8.5 | 0.197 ± 0.026 | -24.5 ± 5.3 |

From Table 7.4 is possible to see the influence of increasing the amount of SPIONs added to the formulation in the size and PI of the nanoparticles, both values increase by increasing the amount of SPIONs. Despite the increase is not large enough to discard the addition of 1 mg, visually it was possible to see the presence of insoluble aggregates after centrifugation. These aggregates were not seen in the nanoparticles produced using 0.5 mg of SPIONs, indicating that LPHNPs encapsulating 1 mg are unstable, leading to aggregation and formation of the insoluble plaques (Guerrini et al., 2018). That way, 0.5 mg is de optimal amount of SPIONs to add to the formulation.

## 7.2. Encapsulation Efficiency (EE)

When using nanoparticles as drug carriers, the amount of drug added to the formulation is known. However, not all drug added to the formulation encapsulates in the nanoparticles. For that reason, it is important to assess the encapsulation efficiency of the encapsulated components in the nanosystem. In this case, the proposed nanosystem encapsulates SPIONs and curcumin.

### 7.2.1. SPIONs

After producing nanoparticles encapsulating SPIONs, they are purified using centrifugation, as explained before. After the centrifugation step, a pellet and a supernatant are

obtained. In the pellet, there are the produced nanoparticles and, in the supernatant, stays the SPIONs that did not encapsulate in the hybrid nanoparticles. For that reason, the EE for SPIONs was obtained by quantifying the amount of SPIONs in the supernatant after the centrifugation cycle.

The obtained results show that 0.131 mg of SPIONs did not encapsulate in the hybrid nanoparticles, meaning that inside the hybrid nanoparticles must be 0.369 mg of SPIONs. The EE for this case is 73.8%.

### 7.2.2. Curcumin

Before the functionalization of the nanoparticles to obtain the proposed nanosystem, only lasts the encapsulation of the chosen drug, curcumin. To optimize its encapsulation, different amounts of curcumin were added to the formulation with SPIONs. The encapsulation efficiency (EE) and drug loading (DL) were calculated for each condition. The results are shown in Table 7.5.

**Table 7.5** Obtained results of EE and DL for the encapsulation of different amounts of curcumin

| Mass of curcumin added to the formulation (mg) | Mass in the supernatant (mg) | Mass inside nanoparticles (mg) | EE (%) | DL (%) |
|---|---|---|---|---|
| 0.500 | 0.032 | 0.468 | 93.6 | 4.7 |
| 1.000 | 0.047 | 0.953 | 95.3 | 9.5 |
| 1.500 | 0.047 | 1.453 | 96.9 | 14.5 |
| 2.000 | 0.046 | 1.954 | 97.7 | 19.5 |

From Table 7.5, it is possible to see that the greater the amount of curcumin added to the formulation, the greater the amount that gets encapsulated. Therefore, as we move down the table, the EE and DL values increase. With these results, it is possible to affirm that the developed nanosystem shows ideal characteristics to encapsulate a hydrophobic drug.

## 7.3. FTIR Spectroscopy

As explained before, until reaching the final PLGA-lecithin hybrid nanoparticles encapsulating SPIONs, it was necessary to reach different stages. The most important ones were PLGA nanoparticles, hybrid nanoparticles, and the hybrid nanoparticles encapsulating SPIONs. To confirm the presence of the added components, analysis of the chemical structure of these nanoparticles were performed using FTIR spectroscopy. The obtained graphics for each stage are shown below in Figure 7.4.

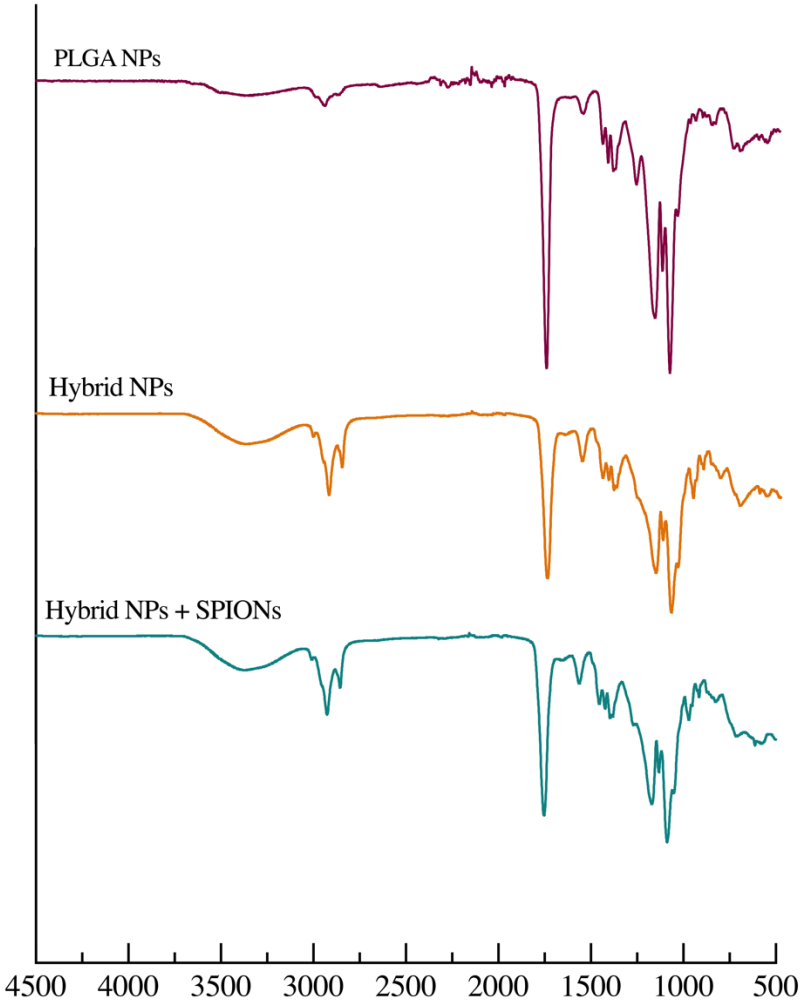


**Figure 7.4** FTIR spectrum of PLGA nanoparticles, hybrid (PLGA+lecithin) nanoparticles and hybrid nanoparticles encapsulating SPIONs.

In the FTIR spectrum of PLGA nanoparticles, it is possible to see a band at 3295 $cm^{-1}$ derived from the stretching of the terminal hydroxyl groups in PLGA and at 2911, 2944 and 2873 $cm^{-1}$ three bands can be observed due to the CH stretching (Mollaeva et al., 2021; Zhang et al., 2016).

At 1754 $cm^{-1}$ it is possible to see the characteristic band of the stretching of the carbonyl groups (Paragkumar N et al., 2006; Zhang et al., 2016). The CH stretching of methyl groups is represented by the band at 1454 $cm^{-1}$, and the bending vibration of the $CH_2$ and $CH(CH_3)$ is represented by the band at 1421 $cm^{-1}$ (Paragkumar N et al., 2006).

Finally, at 1091 and at 1050 $cm^{-1}$ it is possible to see the bands due to C-O-C stretching and C-$CH_3$ stretching, respectively (Lu et al., 2019; Paragkumar N et al., 2006).

Comparing the PLGA nanoparticles FTIR with the hybrid nanoparticles, it is possible to see that the biggest difference is present in the intensity of the three bands located between 2800

and 3000 $cm^{-1}$. This indicates the presence of a higher amount of those vibrations in the sample, in this case due to the presence of lecithin (Oliveira et al., 2012). The FTIR spectrum of lecithin also shows bands at those wavenumbers due to its hydrophobic tail regions. Another difference between the two spectrums is the appearance of a band at 969 $cm^{-1}$ due to $N^{+}(CH_3)_3$ stretching indicating, once more, the presence of lecithin (Tantipolphan et al., 2007).

Finally, comparing the hybrid nanoparticles FTIR to the hybrid nanoparticles + SPIONs FTIR it can be concluded that there is not much difference between the two spectrums. The absence of SPIONs characteristic peaks, namely the peak around 530 $cm^{-1}$ due to Fe-O stretching, can be explained due to the low concentration of SPIONs in the nanoparticles and due to the fact they are encapsulated in the polymeric core (Saengruengrit et al., 2018).

## 7.4. Magnetic Characterization

The magnetic characterization of the LPHNPs encapsulating SPIONs was assessed using SQUID. The results can be seen in Figure 7.5.

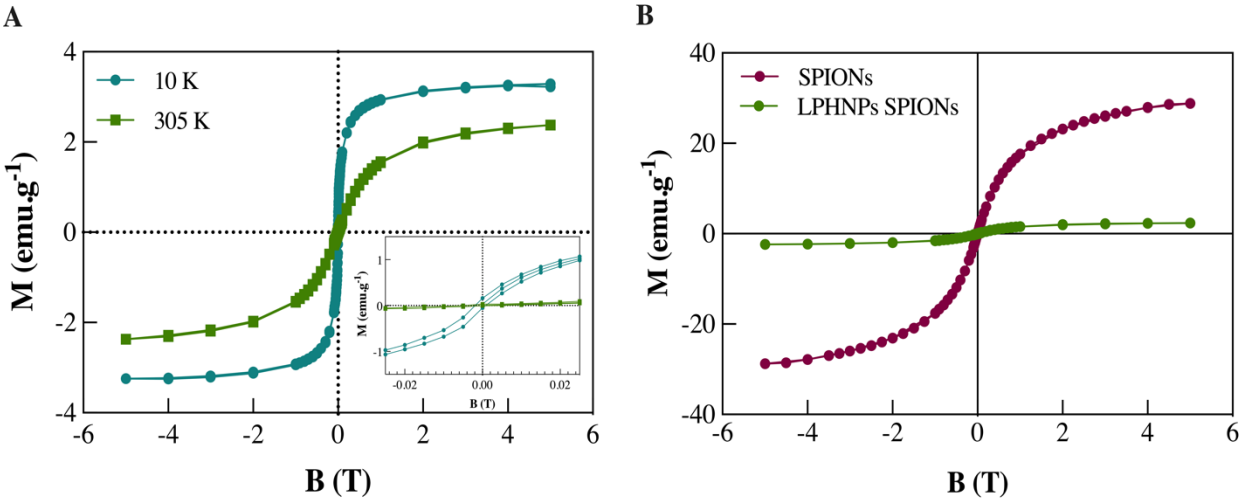


**Figure 7.5** Magnetic characterization of SPIONs encapsulated in PLGA at 10 and 305 K (A) and comparison between the curves obtained for SPIONs and for SPIONs encapsulated in PLGA at 305 K (B).

From Figure 7.5 - (A) it can be seen that LPHNPs encapsulating SPIONs have a higher saturation magnetization at 10 K. This saturation magnetization is 3.3 $emu.g^{-1}$ while for the 305 K this value decreases to 2.3 $emu.g^{-1}$. Nevertheless, from the ampliation seen in the same figure, it is seen that these nanoparticles only show a superparamagnetic behavior at 305 K, with no remanence or coercivity. The nanoparticles at 10 K show a remanence of 0.1 $emu.g^{-1}$ and a coercivity of 10 Oe.

Then, on Figure 7.5 – (B) there is a comparison between the curves of SPIONs and SPIONs encapsulated in LPHNPs. It is clear to see a decrease in the saturation magnetization value when the SPIONs are encapsulated. This decrease is related not only because the SPIONs are encapsulated in the polymeric core, but also because the SPIONs concentration in the hybrid nanoparticles is very low. This influence was already expected since the same relation has already been described. However, with these results, it is possible to affirm that even with the encapsulation in PLGA-lecithin hybrid nanoparticles, the SPIONs do not lose their superparamagnetic behavior (Saengruengrit et al., 2018).

### 7.5. Magnetic Hyperthermia

Magnetic hyperthermia assays of the produced nanoparticles was performed to assess the ability of these particles to produce heat.

The hyperthermia effect consists in increasing the temperature of a tissue, usually to 42ºC. Taking in account the physiological temperature is about 37ºC, to reach the 42ºC the nanoparticles must be able to produce a temperature variation of 5ºC.

With the performed tests, it was possible to conclude that the nanoparticles were not able to induce any temperature variation, indicating this way that they are not able to induce hyperthermia. The results can be explained due to the low amount of SPIONs in the produced nanoparticles.

To make these nanoparticles suitable for magnetic hyperthermia, they should be optimized in order to increase the amount of SPIONs inside the lipid-polymer nanoparticles.

## 8. Functionalization of LPHNPs

### 8.1. EDC/NHS Reaction

The EDC/NHS reaction is widely used as a coupling reaction for nanoparticles. Previously studies performed in our laboratory with similar nanoparticles showed that the step of the activation of the carboxyl group with the EDC and NHS reagents promotes changes to the nanoparticles, affecting their stability.

To avoid that, instead of directly functionalizing the nanoparticles by activating the carboxyl group on their surface, the carboxylic group functionalized will be the one present in the DSPE-PEG-COOH. That way, the peptide will link to the DSPE-PEG-COOH forming DSPE-PEG-CPP that can then be adsorbed into the nanoparticle's surface.

The EDC/NHS reaction was performed by adding 200 µg of CPP to 3 mg of DSPE-PEG-COOH activated. To assess the yield of the reaction the fluorescence of the obtained solution was measured. The fluorescence of the solution is given by the tryptophan present in the CPP. With this, it was possible to see that the yield of the reaction was 13.3 %.

## 8.2. DSPE-PEG-CPP Adsorption

To modify the nanoparticle's surface, the DSPE-PEG-CPP was adsorbed into the nanoparticle's surface by weak interactions (Almeida & Vale, 2022). To assess if the DSPE-PEG-CPP is at the nanoparticle's surface, the nanoparticle size should be measured since the formation of a layer with DSPE-PEG-CPP in the nanoparticle's surface increase the particle size (Almeida & Vale, 2022).

Before the adsorption, the nanoparticles have a particle size of 91.6 ± 1.6 nm and after the adsorption 120.1± 0.1 nm, indicating this way that the adsorption of the DSPE-PEG-CPP into the nanoparticle's surface was successful.

## 8.3. FTIR Spectroscopy of the Nanosystem

To analyze the chemical composition of the final nanosystem the FTIR spectroscopy technique was used. The obtained spectrum for the nanosystem is shown in Figure 8.1.

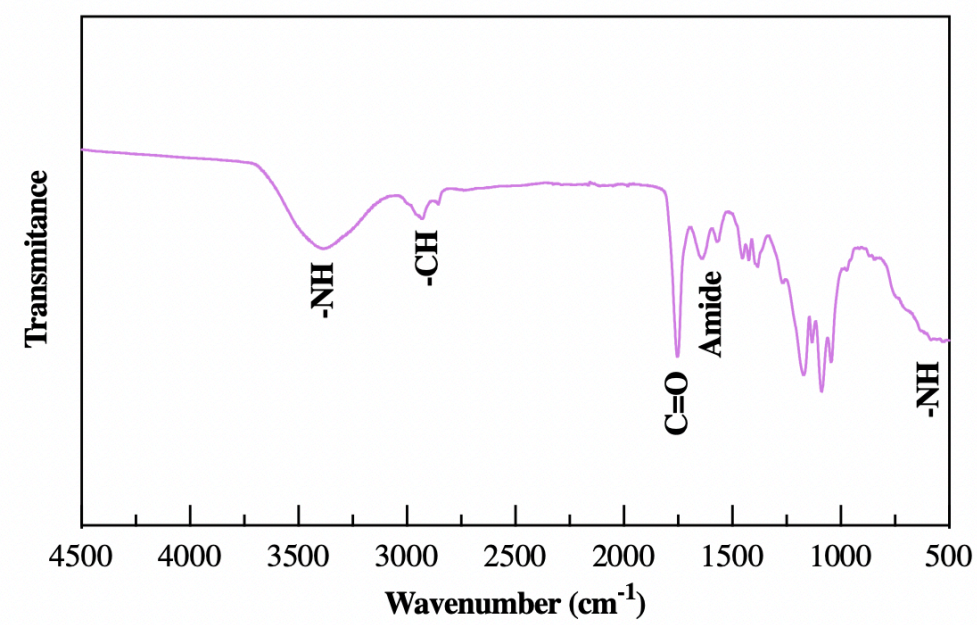


**Figure 8.1** FTIR spectrum of the final nanosystem

From the obtained FTIR spectrum (Figure 8.1) it is possible to identify similar peaks to the ones present in the FTIR spectrum of hybrid nanoparticles + SPIONs. Those peaks are the ones located at 2750-3000 $cm^{-1}$ due to C-H stretching, the peak at 1751 $cm^{-1}$ due to the stretching of carbonyl groups and all the peaks located between 1455 and 900 $cm^{-1}$.

The main differences between the spectrums that indicate the presence of the CPP are the intense band at 3385 $cm^{-1}$ due to N-H stretching, the two bands at 1637 and 1569 $cm^{-1}$ indicating the formation of amide groups and finally the band at 534 $cm^{-1}$ due to N-H out of plan bend (Marasini et al., 2020).

With the evidence obtained from the analysis of the FTIR spectrum of the final nanosystem, it can be concluded that the functionalization of the nanoparticles was successful.

# 9. Internalization of the nanosystem in cultured cells

## 9.1. Cytotoxicity Assays

In order to study the effect of the nanoparticles on cell viability, cytotoxicity assays were performed. Since the main focus of the nanosystem developed is to overcome the BBB, the cells used for the assay are human brain endothelial cells (HBEC-5i cell line). The use of brain endothelial cells for the assay is explained by the fact that endothelial cells constitute the basis of BBB.

These studies were performed for different concentrations of nanoparticles (0.39 to 100 μg/mL) for 24 and 48 h. The results obtained are shown in Figure 9.1.

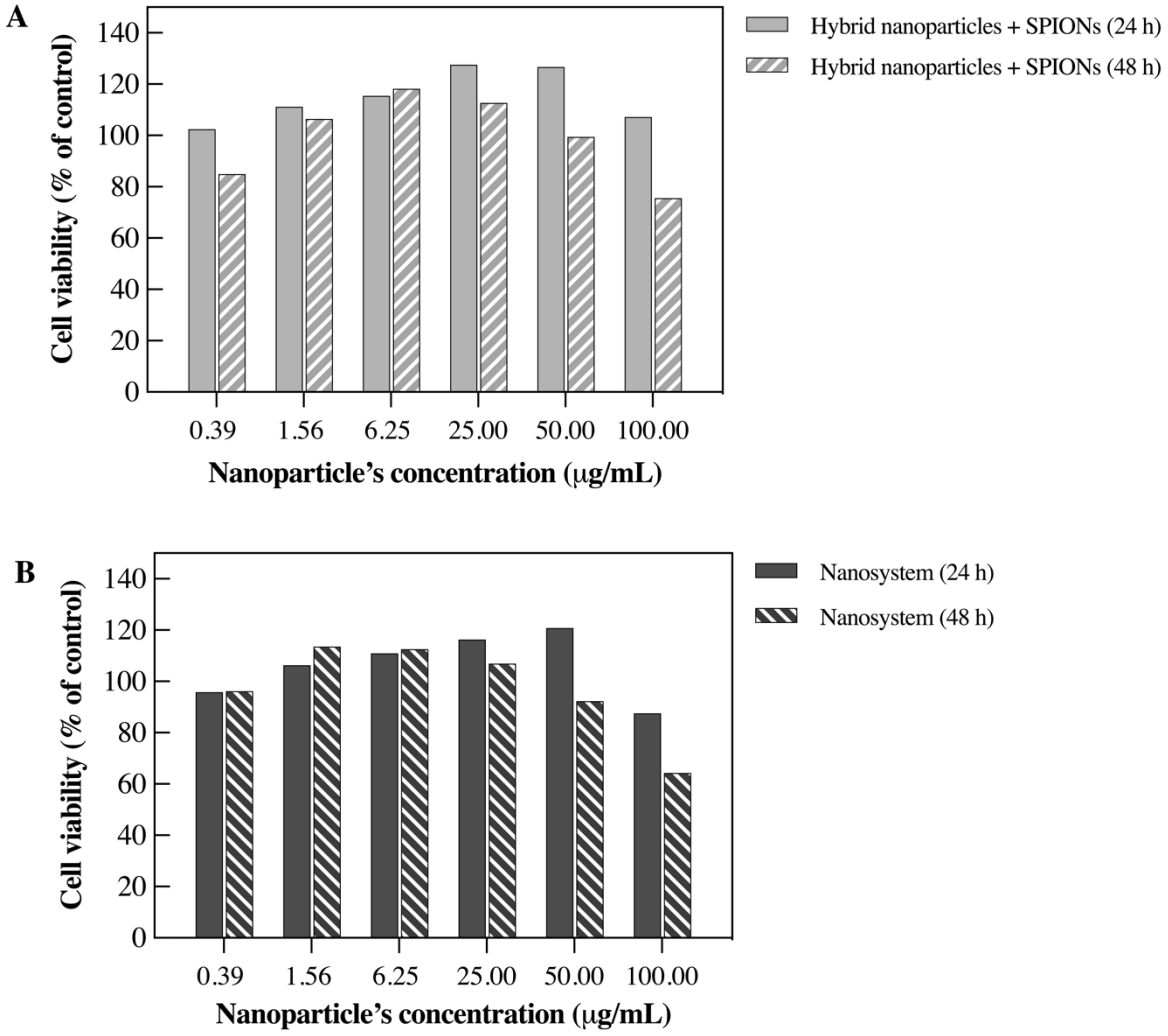


**Figure 9.1** Cell viability of HBEC-5i cell line after 24 and 48 h exposition to (A) Hybrid nanoparticles + SPIONs and (B) Nanosystem. Data is expressed as the average of one independent experiment.

From the graphics, it is possible to see that for both types of nanoparticles the variation in cell viability remains constant with the increase of nanoparticle's concentration at 24 h, except for the nanosystem at a concentration of 100 μg/mL.

Moreover, it can also be seen that after a 48 h incubation the nanoparticles seem to become toxic to the cells at a concentration of 100 μg/mL. All other concentrations did not demonstrate to be toxic to the cells after 48 h.

Further studies should be performed to confirm the obtained results.

## 9.2. Cell exposure to the nanosystem and uptake studies

The flow cytometry technique was used to assess the nanoparticle's internalization in HBEC-5i cell line. For that, two different timepoints were assessed, 30 min to assess the rapid

uptake and 24 h. The nanoparticles were stained with coumarin-6 so they could be detected by the technique. One example of the graphics obtained from the flow cytometry is shown in Figure 9.2.

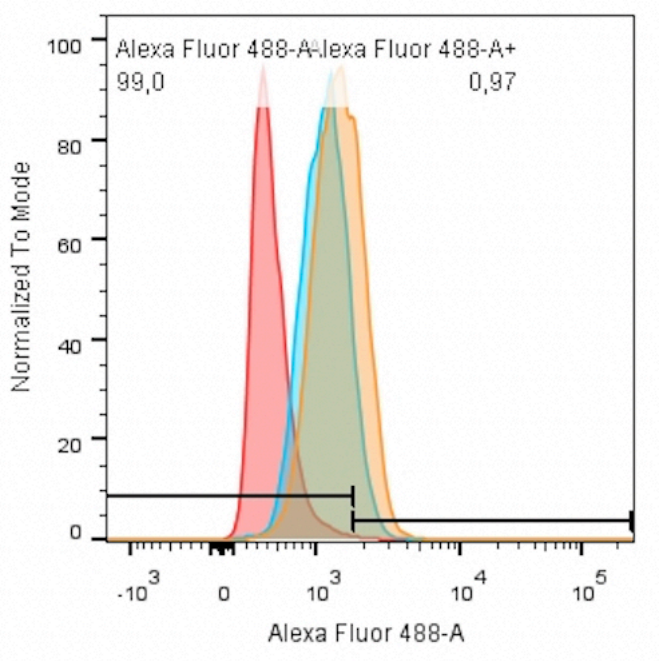


**Figure 9.2 Flow cytometry analysis of nanoparticle's internalization in HBEC cell line.** Red histogram represents the negative control (only the cells); blue histogram represents the cells stained with hybrid nanoparticles + SPIONs (not functionalized with the CPP) and the orange histogram corresponds to the cells labeled with the final nanosystem (functionalized with the CPP).

The technique is based on fluorescence, and for that, it is required to choose the ideal laser to excite the compound that emits fluorescence. In this case, the compound is coumarin-6, as referred before. As it is possible to see from Figure 9.2, there is a black line separating the end of the negative control form the rest of the histogram. The ideal laser would be the one that separates the negative control from the samples to analyze without any overlap of the histograms (i.e. the red histogram should be placed entirely on the left side of the black line separation, and the blue and orange should be mainly on the right) (Schmit et al., 2021). With this, it is possible to conclude that the ideal laser was not the one used to perform the assay since the ideal laser does not exist in the institution where the assay was done. The laser used was chosen by comparing the three different lasers available, and this one was the one with the best settings to perform the assay.

The main purpose of using flow cytometry was to assess the difference in cell uptake that could occur from the nanoparticles non-functionalized to the nanoparticles functionalized in HBEC-5i cell line. Moreover, with the use of different timepoints, it is also possible to assess

the internalization pattern of the nanoparticles in the cells. The obtained results are shown in Figure 9.3.

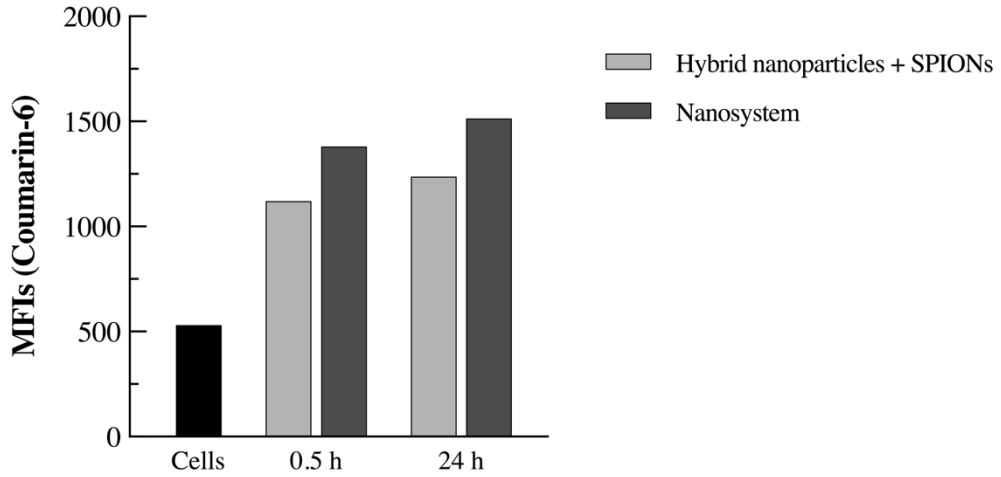


**Figure 9.3** Flow cytometry results of the nanoparticle's uptake by HBEC-5i cells at two different timepoints (0.5 and 24h). Data is expressed as the average of one independent experiment.

From Figure 9.3 it is possible to see that the fluorescence obtained to the control is much lower compared to the fluorescence obtained with the different samples. This indicates that the nanoparticles uptake occurred successfully with the two different types of nanoparticles.

With this, it is also possible to compare the uptake of the two types of nanoparticles by HBEC-5i cells. As is seen in Figure 9.3 the nanosystem (hybrid nanoparticles + SPIONs + CPP) was internalized to a greater extent than the hybrid nanoparticles + SPIONs. This was the expected result since the functionalization of the nanoparticles with the CPP was done with the expectation that it would facilitate the entry of the nanoparticles into the cells.

Moreover, with the experiment it was possible to compare the internalization of the same type of nanoparticles in the two different timepoints. For both types of nanoparticles, it was possible to conclude that increasing the time of cell exposure does not lead to a much higher amount of nanoparticles that internalize in the cells. This way, it is possible to affirm that the nanoparticles are rapidly uptake by cells since they do not show a significant internalization over time.

Higher concentration's range and more timepoints (between 0.5 and 24 h) should be assessed in future studies to confirm this hypothesis. However, it should always be taken into account that the assay was done using a concentration of 25 µg/mL and, according to the data obtained from the cytotoxicity assays, the concentrations tested should never exceed 100 µg/mL.

# Chapter 5

# Concluding Remarks and Future Perspectives

AD is the neurodegenerative disorder with higher impact in dementia all over the world. By 2050, it is expected that 12.7 million people aged 65 and older will be affected by AD. This way AD can be considered a global health problem and, for that reason, there is a huge need to find a treatment able to induce AD regression since until now, the only pharmacologic therapy administered to AD patients only treat symptoms.

One of the main problems in finding the ideal treatment to the disorder is the presence of the BBB that impedes the passage to most molecules with high potential for treating AD.

Recently, nanotechnology was proposed with high potential to overcome the poor permeability of the molecules to the BBB. Because of that, the main goal of this project was to develop a possible therapeutic nanosystem able to overcome the BBB and deliver the chosen drug in the CNS.

In a first stage, SPIONs were synthesized using the thermal decomposition method (a previously optimized protocol in the laboratory) and were characterized to confirm their ideal size and shape for biomedical applications.

Then, the production of lipid-polymer hybrid nanoparticles was optimized to reach the ideal hydrodynamic size for the intended application. The optimized protocol consists in the single emulsion-solvent evaporation method, using SC as surfactant to obtain the nanoparticles composed by a polymeric core of PLGA and a lipid layer of lecithin. Then, the optimization of the SPIONs and curcumin encapsulation was also performed. During the entire optimization, the nanoparticles were always analyzed using FTIR and DLS techniques to assure their composition and hydrodynamic diameter, respectively. After the optimization, the nanoparticles were further analyzed by SQUID technique that showed the superparamagnetic behavior of the nanoparticles at 305 K. The capacity of the nanoparticles to generate heat (magnetic hyperthermia) was also assessed; however, due to the low concentration of SPIONs,

the nanosystem was not able to generate heat. This way, the produced nanosystem cannot be used for magnetic hyperthermia purposes.

In this master thesis the strategy adopted to increase the permeability of the nanoparticles through the BBB was to functionalize their surface using a peptide able to translocate cell membranes, named CPP. To promote the linkage between the nanoparticle's surface and the CPP the EDC/NHS reaction was used. The reaction promoted the formation of amide bonds between the carboxyl groups in the nanoparticles and amine groups of the CPP.

After the functionalization, final nanosystem was obtained. The nanosystem was characterized by DLS technique to assess the hydrodynamic diameter. The result obtained showed a nanosystem of 120.1 ± 0.1 nm. The FTIR technique was used to characterize the nanosystem and to confirm the presence of the CPP.

Since the main goal of the master thesis was to develop a nanosystem able to cross the BBB, cellular assays were performed to assess the efficiency of the nanosystem to internalize in human microvascular endothelial cells. First, cytotoxicity studies were performed to assess the ideal concentration of nanoparticles to use. Then, the capacity of the nanoparticles in internalizing in cells was assessed using the previously determined concentration of nanoparticles. The results were obtained using the flow cytometry technique and it was possible to conclude that the nanoparticles tested were able to internalize in HBEC-5i cells. It was also observed that, comparing the internalization of the hybrid nanoparticles + SPIONs not functionalized with the nanosystem (functionalized), the CPP showed a positive impact in the internalization since the nanosystem was the most uptake by the cells, as expected.

In general, the proposed goals for the project were accomplished. The designed nanosystem was produced with the ideal characteristics for a biomedical application, and especially for crossing the BBB. Also, the cellular assays showed its capacity to be uptake by endothelial cells *in vitro*.

In the future, further studies should be done to confirm the tendency observed in the cellular assays, since they were only performed once. Ideally, transwell assays should be done since they better mimetic the BBB when compared to the performed *in vitro* assay. Then, the drug release profile of curcumin should also be assessed. Finally, to use the developed nanosystem for magnetic hyperthermia purposes, the concentration of SPIONs in the nanosystem should also be increased.

# References


Abbott, N. J., Patabendige, A. A. K., Dolman, D. E. M., Yusof, S. R., & Begley, D. J. (2010). Structure and function of the blood-brain barrier. *Neurobiology of Disease*, *37*(1), 13–25.

Abdel Aziz, O. A., Arafa, K., Abo Dena, A. S., & El-sherbiny, I. M. (2020). Superparamagnetic Iron Oxide Nanoparticles (SPIONs): Preparation and Recent Applications. *Journal of Nanotechnology and Advanced Materials*, *8*(1), 21–29.

Ahlschwede, K. M., Curran, G. L., Rosenberg, J. T., Grant, S. C., Sarkar, G., Jenkins, R. B., Ramakrishnan, S., Poduslo, J. F., & Kandimalla, K. K. (2019). Cationic carrier peptide enhances cerebrovascular targeting of nanoparticles in Alzheimer's disease brain. *Nanomedicine: Nanotechnology, Biology, and Medicine*, *16*, 258–266.

Almeida, J., & Vale, N. (2022). *Development of Neuropeptide Y and Cell-Penetrating Peptide MAP Adsorbed onto Lipid Nanoparticle Surface*.

Amo, L. Del, Cano, A., Ettcheto, M., Souto, E. B., Espina, M., Camins, A., García, M. L., & Sánchez-López, E. (2021). Surface functionalization of plga nanoparticles to increase transport across the bbb for alzheimer's disease. *Applied Sciences (Switzerland)*, *11*(9).

Ausó, E., Gómez-Vicente, V., & Esquiva, G. (2020). Biomarkers for alzheimer's disease early diagnosis. *Journal of Personalized Medicine*, *10*(3), 1–27.

Barbosa, M., Martins, M. C. L., & Gomes, P. (2015). Grafting techniques towards production of peptide-tethered hydrogels, a novel class of materials with biomedical interest. *Gels*, *1*(2), 194–218.

Bartczak, D., & Kanaras, A. G. (2011). Preparation of peptide-functionalized gold nanoparticles using one pot EDC/Sulfo-NHS coupling. *Langmuir*, *27*(16), 10119–10123.

Bhat, A., Mahalakshmi, A. M., Ray, B., Tuladhar, S., Hediyal, T. A., Manthiannem, E., Padamati, J., Chandra, R., Chidambaram, S. B., & Sakharkar, M. K. (2019). Benefits of curcumin in brain disorders. *BioFactors*, *45*(5), 666–689.

Bose, R. J. C., Lee, S. H., & Park, H. (2016). Lipid-based surface engineering of PLGA nanoparticles for drug and gene delivery applications. *Biomaterials Research*, *20*(1), 1–9.

Bose, R. J. C., Ravikumar, R., Karuppagounder, V., Bennet, D., Rangasamy, S., & Thandavarayan, R. A. (2017). Lipid–polymer hybrid nanoparticle-mediated therapeutics delivery: advances and challenges. *Drug Discovery Today*, *22*(8), 1258–1265.

Carvalho, P. M., Felício, M. R., Santos, N. C., Gonçalves, S., & Domingues, M. M. (2018). Application of light scattering techniques to nanoparticle characterization and development. *Frontiers in Chemistry*, *6*(June), 1–17.

Ceña, V., & Játiva, P. (2018). Nanoparticle crossing of blood-brain barrier: A road to new therapeutic approaches to central nervous system diseases. *Nanomedicine*, *13*(13), 1513–1516.

Chen, J., Zhang, C., Liu, Q., Shao, X., Feng, C., Shen, Y., Zhang, Q., & Jiang, X. (2012). Solanum tuberosum lectin-conjugated PLGA nanoparticles for nose-to-brain delivery: In

vivo and in vitro evaluations. *Journal of Drug Targeting*, *20*(2), 174–184.

Chen, M., Du, Z. Y., Zheng, X., Li, D. L., Zhou, R. P., & Zhang, K. (2018). Use of curcumin in diagnosis, prevention, and treatment of Alzheimer's disease. *Neural Regeneration Research*, *13*(4), 742–752.

Cheow, W. S., & Hadinoto, K. (2011). Factors affecting drug encapsulation and stability of lipid-polymer hybrid nanoparticles. *Colloids and Surfaces B: Biointerfaces*, *85*(2), 214–220.

Chin, D., Huebbe, P., Pallauf, K., & Rimbach, G. (2013). Neuroprotective Properties of Curcumin in Alzheimer's Disease – Merits and Limitations. *Current Medicinal Chemistry*, *20*(32), 3955–3985.

Choi, J. S., Cao, J., Naeem, M., Noh, J., Hasan, N., Choi, H. K., & Yoo, J. W. (2014). Size-controlled biodegradable nanoparticles: Preparation and size-dependent cellular uptake and tumor cell growth inhibition. *Colloids and Surfaces B: Biointerfaces*, *122*, 545–551.

Ćirin, D. M., Poša, M. M., & Krstonošić, V. S. (2012). Interactions between sodium cholate or sodium deoxycholate and nonionic surfactant (Tween 20 or Tween 60) in aqueous solution. *Industrial and Engineering Chemistry Research*, *51*(9), 3670–3676.

Dadfar, S. M., Roemhild, K., Drude, N. I., von Stillfried, S., Knüchel, R., Kiessling, F., & Lammers, T. (2019). Iron oxide nanoparticles: Diagnostic, therapeutic and theranostic applications. *Advanced Drug Delivery Reviews*, *138*, 302–325.

Dave, V., Tak, K., Sohgaura, A., Gupta, A., Sadhu, V., & Reddy, K. R. (2019). Lipid-polymer hybrid nanoparticles: Synthesis strategies and biomedical applications. *Journal of Microbiological Methods*, *160*(March), 130–142.

De-Paula, V. J., Radanovic, M., Diniz, B. S., & Forlenza, O. V. (2012). Alzheimer's Disease. *Protein Aggregation and Fibrillogenesis in Cerebral and Systemic Amyloid Disease*, *65*, 389–455.

de Lima, L. S., & Mortari, M. R. (2022). Therapeutic nanoparticles in the brain: A review of types, physicochemical properties and challenges. *International Journal of Pharmaceutics*, *612*(July 2021).

Deatsch, A. E., & Evans, B. A. (2014). Heating efficiency in magnetic nanoparticle hyperthermia. *Journal of Magnetism and Magnetic Materials*, *354*, 163–172.

Deok Kong, S., Sartor, M., Jack Hu, C. M., Zhang, W., Zhang, L., & Jin, S. (2013). Magnetic field activated lipid-polymer hybrid nanoparticles for stimuli-responsive drug release. *Acta Biomaterialia*, *9*(3), 5447–5452.

Deshmukh, R., Wagh, P., & Naik, J. (2016). Solvent evaporation and spray drying technique for micro- and nanospheres/particles preparation: A review. *Drying Technology*, *34*(15), 1758–1772.

Dulińska-Litewka, J., Łazarczyk, A., Hałubiec, P., Szafrański, O., Karnas, K., & Karewicz, A. (2019). Superparamagnetic iron oxide nanoparticles-current and prospective medical applications. *Materials*, *12*(4).

Dyne, E., Prakash, P. S., Li, J., Yu, B., Schmidt, T. L., Huang, S., & Kim, M. H. (2021). Mild magnetic nanoparticle hyperthermia promotes the disaggregation and microglia-mediated clearance of beta-amyloid plaques. *Nanomedicine: Nanotechnology, Biology, and Medicine*, *34*, 102397.

Elmeshad, A. N., & Tadros, M. I. (2011). Transdermal delivery of an anti-cancer drug via W/O emulsions based on alkyl polyglycosides and lecithin: Design, characterization, and in vivo evaluation of the possible irritation potential in rats. *AAPS PharmSciTech*, *12*(1), 1–9.

Esim, O., Bakirhan, N. K., Sarper, M., Savaser, A., Ozkan, S. A., & Ozkan, Y. (2020). Influence of emulsifiers on the formation and in vitro anticancer activity of epirubicin loaded PLGA nanoparticles. *Journal of Drug Delivery Science and Technology*, *60*(January), 102027.

Faghihzadeh, F., Anaya, N. M., Schifman, L. A., & Oyanedel-Craver, V. (2016). Fourier transform infrared spectroscopy to assess molecular-level changes in microorganisms exposed to nanoparticles. *Nanotechnology for Environmental Engineering*, *1*(1), 1–16.

Fan, S., Zheng, Y., Liu, X., Fang, W., Chena, X., Liao, W., Jing, X., Lei, M., Tao, E., Ma, Q., Zhang, X., Guo, R., & Liu, J. (2018). Curcumin-loaded PLGA-PEG nanoparticles conjugated with B6 peptide for potential use in Alzheimer's disease. *Drug Delivery*, *25*(1), 1044–1055.

Farkhondeh, T., Samarghandian, S., Pourbagher-Shahri, A. M., & Sedaghat, M. (2019). The impact of curcumin and its modified formulations on Alzheimer's disease. *Journal of Cellular Physiology*, *234*(10), 16953–16965.

Fazakas, C., Wilhelm, I., Nagyoszi, P., Farkas, A. E., Haskó, J., Molnár, J., Bauer, H., Bauer, H. C., Ayaydin, F., Dung, N. T. K., Siklós, L., & Krizbai, I. A. (2011). Transmigration of melanoma cells through the blood-brain barrier: Role of endothelial tight junctions and melanoma-released serine proteases. *PLoS ONE*, *6*(6).

Feltrin, F. da S., Agner, T., Sayer, C., & Lona, L. M. F. (2022). Curcumin encapsulation in functional PLGA nanoparticles: A promising strategy for cancer therapies. *Advances in Colloid and Interface Science*, *300*, 102582.

G. Nava-Arzaluz, M., Pinon-Segundo, E., Ganem-Rondero, A., & Lechuga-Ballesteros, D. (2012). Single Emulsion-Solvent Evaporation Technique and Modifications for the Preparation of Pharmaceutical Polymeric Nanoparticles. *Recent Patents on Drug Delivery & Formulation*, *6*(3), 209–223.

Gaspar, A. S., Santos, P. H. C., Borges, O., Costa, B. F. O., & Durães, L. (2019). Biocompatible and high-magnetically responsive iron oxide nanoparticles for protein loading. *Journal of Physics and Chemistry of Solids*, *134*, 273–285.

Ghitman, J., Biru, E. I., Stan, R., & Iovu, H. (2020). Review of hybrid PLGA nanoparticles: Future of smart drug delivery and theranostics medicine. *Materials and Design*, *193*, 108805.

Gong, Y. K., & Winnik, F. M. (2012). Strategies in biomimetic surface engineering of nanoparticles for biomedical applications. *Nanoscale*, *4*(2), 360–368.

Guerrini, L., Alvarez-Puebla, R. A., & Pazos-Perez, N. (2018). Surface modifications of nanoparticles for stability in biological fluids. *Materials*, *11*(7), 1–28.

Hane, F. T., Lee, B. Y., & Leonenko, Z. (2017). Recent Progress in Alzheimer's Disease Research, Part 1: Pathology. *Journal of Alzheimer's Disease*, *57*(1), 1–28.

Hersh, A. M., Alomari, S., & Tyler, B. M. (2022). Crossing the Blood-Brain Barrier: Advances in Nanoparticle Technology for Drug Delivery in Neuro-Oncology. *International Journal of Molecular Sciences*, *23*(8).

Jardim, K. V., Siqueira, J. L. N., Báo, S. N., Sousa, M. H., & Parize, A. L. (2020). The role of the lecithin addition in the properties and cytotoxic activity of chitosan and chondroitin sulfate nanoparticles containing curcumin. *Carbohydrate Polymers*, *227*(February 2019), 115351.

Jazayeri, M. H., Amani, H., Pourfatollah, A. A., Pazoki-Toroudi, H., & Sedighimoghaddam, B. (2016). Various methods of gold nanoparticles (GNPs) conjugation to antibodies. *Sensing and Bio-Sensing Research*, *9*, 17–22.

Jenjob, R., Phakkeeree, T., Seidi, F., Theerasilp, M., & Crespy, D. (2019). Emulsion Techniques for the Production of Pharmacological Nanoparticles. *Macromolecular Bioscience*, *19*(6), 1–13.

Jun, Y. W., Seo, J. W., & Cheon, J. (2008). Nanoscaling laws of magnetic nanoparticles and their applicabilities in biomedical sciences. *Accounts of Chemical Research*, *41*(2), 179–189.

Khan, H., Yerramilli, A. S., D'Oliveira, A., Alford, T. L., Boffito, D. C., & Patience, G. S. (2020). Experimental methods in chemical engineering: X-ray diffraction spectroscopy—XRD. *Canadian Journal of Chemical Engineering*, *98*(6), 1255–1266.

Kim, S. H., Lee, C. M., & Kafle, K. (2013). Characterization of crystalline cellulose in biomass: Basic principles, applications, and limitations of XRD, NMR, IR, Raman, and SFG. *Korean Journal of Chemical Engineering*, *30*(12), 2127–2141.

Kircher, D. A., Silvis, M. R., Cho, J. H., & Holmen, S. L. (2016). Melanoma brain metastasis: Mechanisms, models, and medicine. *International Journal of Molecular Sciences*, *17*(9).

Kurtan, U., Erdemi, H., Baykal, A., & Güngüneş, H. (2016). Synthesis and magneto-electrical properties of MFe2O4 (Co, Zn) nanoparticles by oleylamine route. *Ceramics International*, *42*(12), 13350–13358.

Kurtan, U., Güngüneş, H., Sözeri, H., & Baykal, A. (2016). Synthesis and characterization of monodisperse NiFe2O4 nanoparticles. *Ceramics International*, *42*(7), 7987–7992.

Lane, C. A., Hardy, J., & Schott, J. M. (2018). Alzheimer's disease. *European Journal of Neurology*, *25*(1), 59–70.

Le, N. T. T., Cao, V. Du, Nguyen, T. N. Q., Le, T. T. H., Tran, T. T., & Thi, T. T. H. (2019). Soy lecithin-derived liposomal delivery systems: Surface modification and current applications. *International Journal of Molecular Sciences*, *20*(19).

Lee, J. S., Cha, J. M., Yoon, H. Y., Lee, J. K., & Kim, Y. K. (2015). Magnetic multi-granule

nanoclusters: A model system that exhibits universal size effect of magnetic coercivity. *Scientific Reports*, *5*(January), 1–7.

Legrand, P., Lesieur, S., Bochot, A., Gref, R., Raatjes, W., Barratt, G., & Vauthier, C. (2007). Influence of polymer behaviour in organic solution on the production of polylactide nanoparticles by nanoprecipitation. *International Journal of Pharmaceutics*, *344*(1–2), 33–43.

Li, K., Nejadnik, H., & Daldrup-Link, H. E. (2017). Next-generation superparamagnetic iron oxide nanoparticles for cancer theranostics. *Drug Discovery Today*, *22*(9), 1421–1429.

Li, X., Tsibouklis, J., Weng, T., Zhang, B., Yin, G., Feng, G., Cui, Y., Savina, I. N., Mikhalovska, L. I., Sandeman, S. R., Howel, C. A., & Mikhalovsky, S. V. (2017). Nano carriers for drug transport across the blood–brain barrier. *Journal of Drug Targeting*, *25*(1), 17–28.

Lin, Y., Zhou, M., Tai, X., Li, H., Han, X., & Yu, J. (2021). Analytical transmission electron microscopy for emerging advanced materials. *Matter*, *4*(7), 2309–2339.

Liu, L., Zhang, X., Li, W., Sun, H., Lou, Y., Zhang, X., & Li, F. (2013). Transferrin receptor antibody-modified α-cobrotoxin-loaded nanoparticles enable drug delivery across the blood-brain barrier by intranasal administration. *Journal of Nanoparticle Research*, *15*(11).

Liu, Y., Pan, J., & Feng, S. S. (2010). Nanoparticles of lipid monolayer shell and biodegradable polymer core for controlled release of paclitaxel: Effects of surfactants on particles size, characteristics and in vitro performance. *International Journal of Pharmaceutics*, *395*(1–2), 243–250.

Lopes, R., Eleutério, C. V., Gonalves, L. M. D., Cruz, M. E. M., & Almeida, A. J. (2012). Lipid nanoparticles containing oryzalin for the treatment of leishmaniasis. *European Journal of Pharmaceutical Sciences*, *45*(4), 442–450.

López-Lorente, Á. I., & Mizaikoff, B. (2016). Recent advances on the characterization of nanoparticles using infrared spectroscopy. *TrAC - Trends in Analytical Chemistry*, *84*, 97–106.

Lowery, F. J., & Yu, D. (2017). Brain metastasis: Unique challenges and open opportunities. *Biochimica et Biophysica Acta - Reviews on Cancer*, *1867*(1), 49–57.

Lu, B., Lv, X., & Le, Y. (2019). Chitosan-modified PLGA nanoparticles for control-released drug delivery. *Polymers*, *11*(2).

Luissint, A. C., Artus, C., Glacial, F., Ganeshamoorthy, K., & Couraud, P. O. (2012). Tight junctions at the blood brain barrier: Physiological architecture and disease-associated dysregulation. *Fluids and Barriers of the CNS*, *9*(1), 1–12.

Mandal, B., Bhattacharjee, H., Mittal, N., Sah, H., Balabathula, P., Thoma, L. A., & Wood, G. C. (2013). Core-shell-type lipid-polymer hybrid nanoparticles as a drug delivery platform. *Nanomedicine: Nanotechnology, Biology, and Medicine*, *9*(4), 474–491.

Marasini, R., Nguyen, T. D. T., Rayamajhi, S., & Aryal, S. (2020). Synthesis and characterization of a tumor-seeking LyP-1 peptide integrated lipid-polymer composite

nanoparticle. *Materials Advances*, *1*(3), 469–480.

Martínez Rivas, C. J., Tarhini, M., Badri, W., Miladi, K., Greige-Gerges, H., Nazari, Q. A., Galindo Rodríguez, S. A., Román, R. Á., Fessi, H., & Elaissari, A. (2017). Nanoprecipitation process: From encapsulation to drug delivery. *International Journal of Pharmaceutics*, *532*(1), 66–81.

Matos, J. C., Clara Gonçalves, M., Pereira, L. C. J., Vieira, B. J. C., & Waerenborgh, J. C. (2019). SPIONS prepared in air through improved synthesis methodology: The influence of γ-Fe2O3/Fe3O4 ratio and coating composition on magnetic properties. *Nanomaterials*, *9*(7).

Miguel, M. G., Lourenço, J. P., & Faleiro, M. L. (2020). Superparamagnetic iron oxide nanoparticles and essential oils: A new tool for biological applications. *International Journal of Molecular Sciences*, *21*(18), 1–24.

Miladi, K., Ibraheem, D., Iqbal, M., Sfar, S., Fessi, H., & Elaissari, A. (2014). Particles from preformed polymers as carriers for drug delivery. *EXCLI Journal*, *13*, 28–57.

Mollaeva, M. R., Yabbarov, N., Sokol, M., Chirkina, M., Mollaev, M. D., Zabolotskii, A., Seregina, I., Bolshov, M., Kaplun, A., & Nikolskaya, E. (2021). Optimization, characterization and pharmacokinetic study of meso-tetraphenylporphyrin metal complex-loaded plga nanoparticles. *International Journal of Molecular Sciences*, *22*(22).

Mukherjee, A., Waters, A. K., Kalyan, P., Achrol, A. S., Kesari, S., & Yenugonda, V. M. (2019). Lipid-polymer hybrid nanoparticles as a nextgeneration drug delivery platform: State of the art, emerging technologies, and perspectives. *International Journal of Nanomedicine*, *14*, 1937–1952.

Murdock, R. C., Braydich-Stolle, L., Schrand, A. M., Schlager, J. J., & Hussain, S. M. (2008). Characterization of nanomaterial dispersion in solution prior to in vitro exposure using dynamic light scattering technique. *Toxicological Sciences*, *101*(2), 239–253.

Nelson, N., Port, J., & Pandey, M. (2020). Use of Superparamagnetic Iron Oxide Nanoparticles (SPIONs) via Multiple Imaging Modalities and Modifications to Reduce Cytotoxicity: An Educational Review. *Journal of Nanotheranostics*, *1*(1), 105–135.

Neuberger, T., Schöpf, B., Hofmann, H., Hofmann, M., & Von Rechenberg, B. (2005). Superparamagnetic nanoparticles for biomedical applications: Possibilities and limitations of a new drug delivery system. *Journal of Magnetism and Magnetic Materials*, *293*(1), 483–496.

Obermeier, B., Verma, A., & Ransohoff, R. M. (2016). The blood-brain barrier. *Handbook of Clinical Neurology*, *133*, 39–59.

Oliveira, R. R., Ferreira, F. S., Cintra, E. R., Branquinho, L. C., Bakuzis, A. F., & Lima, E. M. (2012). Magnetic nanoparticles and rapamycin encapsulated into polymeric nanocarriers. *Journal of Biomedical Nanotechnology*, *8*(2), 193–201.

Paragkumar N, T., Edith, D., & Six, J. L. (2006). Surface characteristics of PLA and PLGA films. *Applied Surface Science*, *253*(5), 2758–2764.

Pardridge, W. M. (2005). The blood-brain barrier: Bottleneck in brain drug development.

*NeuroRx*, *2*(1), 3–14.

Peña-Bahamonde, J., Nguyen, H. N., Fanourakis, S. K., & Rodrigues, D. F. (2018). Recent advances in graphene-based biosensor technology with applications in life sciences. *Journal of Nanobiotechnology*, *16*(1), 1–17.

Perez De Berti, I. O., Cagnoli, M. V., Pecchi, G., Alessandrini, J. L., Stewart, S. J., Bengoa, J. F., & Marchetti, S. G. (2013). Alternative low-cost approach to the synthesis of magnetic iron oxide nanoparticles by thermal decomposition of organic precursors. *Nanotechnology*, *24*(17).

Persano, F., Gigli, G., & Leporatti, S. (2021). Lipid-polymer hybrid nanoparticles in cancer therapy: current overview and future directions. *Nano Express*, *2*(1), 012006.

Porsteinsson, A. P., Isaacson, R. S., Knox, S., Sabbagh, M. N., & Rubino, I. (2021). Diagnosis of Early Alzheimer's Disease: Clinical Practice in 2021. *Journal of Prevention of Alzheimer's Disease*, *8*(3), 371–386.

Profaci, C. P., Munji, R. N., Pulido, R. S., & Daneman, R. (2020). The blood–brain barrier in health and disease: Important unanswered questions. *Journal of Experimental Medicine*, *217*(4), 1–16.

Pustulka, K. M., Wohl, A. R., Lee, H. S., Michel, A. R., Han, J., Hoye, T. R., McCormick, A. V., Panyam, J., & Macosko, C. W. (2013). Flash nanoprecipitation: Particle structure and stability. *Molecular Pharmaceutics*, *10*(11), 4367–4377.

Querfurth, H. W., & Laferla, F. M. (2010). Mechanisms of disease: Alzheimer's Disease. *The New England Journal of Medicine*, 329–344.

Raghav, R., & Srivastava, S. (2016). Immobilization strategy for enhancing sensitivity of immunosensors: L-Asparagine-AuNPs as a promising alternative of EDC-NHS activated citrate-AuNPs for antibody immobilization. *Biosensors and Bioelectronics*, *78*, 396–403.

Ramalho, M. J., Sevin, E., Gosselet, F., Lima, J., Coelho, M. A. N., Loureiro, J. A., & Pereira, M. C. (2018). Receptor-mediated PLGA nanoparticles for glioblastoma multiforme treatment. *International Journal of Pharmaceutics*, *545*(1–2), 84–92.

Ramos, A. P. (2017). Dynamic Light Scattering Applied to Nanoparticle Characterization. In *Nanocharacterization Techniques*. Elsevier Inc.

Rampino, A., Borgogna, M., Blasi, P., Bellich, B., & Cesàro, A. (2013). Chitosan nanoparticles: Preparation, size evolution and stability. *International Journal of Pharmaceutics*, *455*(1–2), 219–228.

Saengruengrit, C., Ritprajak, P., Wanichwecharungruang, S., Sharma, A., Salvan, G., Zahn, D. R. T., & Insin, N. (2018). The combined magnetic field and iron oxide-PLGA composite particles: Effective protein antigen delivery and immune stimulation in dendritic cells. *Journal of Colloid and Interface Science*, *520*, 101–111.

Salunkhe, A. B., Khot, V. M., & Pawar, S. H. (2014). Magnetic Hyperthermia with Magnetic Nanoparticles: A Status Review. *Current Topics in Medicinal Chemistry*, *14*(5), 572–594.

Salvador, M., Moyano, A., Martínez-García, J. C., Blanco-López, M. C., & Rivas, M. (2019).

Synthesis of Superparamagnetic Iron Oxide Nanoparticles: SWOT Analysis Towards Their Conjugation to Biomolecules for Molecular Recognition Applications. *Journal of Nanoscience and Nanotechnology*, *19*(8), 4839–4856.

Scheltens, P., Blennow, K., Breteler, M. M. B., de Strooper, B., Frisoni, G. B., Salloway, S., & Van der Flier, W. M. (2016). Alzheimer's disease. *The Lancet*, *388*(10043), 505–517.

Schmit, T., Klomp, M., & Khan, M. N. (2021). An Overview of Flow Cytometry: Its Principles and Applications in Allergic Disease Research. In *Methods in Molecular Biology* (Vol. 2223).

Schneider, M. G. M., Martín, M. J., Otarola, J., Vakarelska, E., Simeonov, V., Lassalle, V., & Nedyalkova, M. (2022). Biomedical Applications of Iron Oxide Nanoparticles: Current Insights Progress and Perspectives. *Pharmaceutics*, *14*(1).

Shabbir, U., Rubab, M., Tyagi, A., & Oh, D. H. (2021). Curcumin and its derivatives as theranostic agents in alzheimer's disease: The implication of nanotechnology. *International Journal of Molecular Sciences*, *22*(1), 1–23.

Shah, S. P., & Misra, A. (2004). Development of liposomal Amphotericin B dry powder inhaler formulation. *Drug Delivery: Journal of Delivery and Targeting of Therapeutic Agents*, *11*(4), 247–253.

Sharifi, I., Shokrollahi, H., & Amiri, S. (2012). Ferrite-based magnetic nanofluids used in hyperthermia applications. *Journal of Magnetism and Magnetic Materials*, *324*(6), 903–915.

Silva, S., Almeida, A. J., & Vale, N. (2019). Combination of cell-penetrating peptides with nanoparticles for therapeutic application: A review. *Biomolecules*, *9*(1).

Soares, P. I. P., Alves, A. M. R., Pereira, L. C. J., Coutinho, J. T., Ferreira, I. M. M., Novo, C. M. M., & Borges, J. P. M. R. (2014). Effects of surfactants on the magnetic properties of iron oxide colloids. *Journal of Colloid and Interface Science*, *419*, 46–51.

Soares, P. I. P., Lochte, F., Echeverria, C., Pereira, L. C. J., T Coutinho, J., Ferreira, I. M. M., Novo, C. M. M., & Borges, J. P. M. R. (2015). Thermal and magnetic properties of iron oxide colloids: Influence of surfactants. *Nanotechnology*, *26*(42).

Sodipo, B. K., & Aziz, A. A. (2016). Recent advances in synthesis and surface modification of superparamagnetic iron oxide nanoparticles with silica. *Journal of Magnetism and Magnetic Materials*, *416*, 275–291.

Song, H. Q., Fan, Y., Hu, Y., Cheng, G., & Xu, F. J. (2021). Polysaccharide–Peptide Conjugates: A Versatile Material Platform for Biomedical Applications. *Advanced Functional Materials*, *31*(6).

Soria Lopez, J. A., González, H. M., & Léger, G. C. (2019). Alzheimer's disease. *Handbook of Clinical Neurology*, *167*, 231–255.

Stephen, Z. R., Kievit, F. M., & Zhang, M. (2011). Magnetite nanoparticles for medical MR imaging. *Materials Today*, *14*(7–8), 330–338.

Su, X., Wang, Z., Li, L., Zheng, M., Zheng, C., Gong, P., Zhao, P., Ma, Y., Tao, Q., & Cai, L.

(2013). Lipid-polymer nanoparticles encapsulating doxorubicin and 2′-deoxy-5-azacytidine enhance the sensitivity of cancer cells to chemical therapeutics. *Molecular Pharmaceutics*, *10*(5), 1901–1909.

Sweeney, M. D., Sagare, A. P., & Zlokovic, B. V. (2018). Blood-brain barrier breakdown in Alzheimer disease and other neurodegenerative disorders. *Nature Reviews Neurology*, *14*(3), 133–150.

Tantipolphan, R., Rades, T., McQuillan, A. J., & Medlicott, N. J. (2007). Adsorption of bovine serum albumin (BSA) onto lecithin studied by attenuated total reflectance Fourier transform infrared (ATR-FTIR) spectroscopy. *International Journal of Pharmaceutics*, *337*(1–2), 40–47.

Titus, D., James Jebaseelan Samuel, E., & Roopan, S. M. (2019). Nanoparticle characterization techniques. In *Green Synthesis, Characterization and Applications of Nanoparticles*. Elsevier Inc.

Tsou, Y. H., Zhang, X. Q., Zhu, H., Syed, S., & Xu, X. (2017). Drug Delivery to the Brain across the Blood–Brain Barrier Using Nanomaterials. *Small*, *13*(43), 1–17.

Turcheniuk, K., Tarasevych, A. V., Kukhar, V. P., Boukherroub, R., & Szunerits, S. (2013). Recent advances in surface chemistry strategies for the fabrication of functional iron oxide based magnetic nanoparticles. *Nanoscale*, *5*(22), 10729–10752.

Vale, N., Duarte, D., Silva, S., Correia, A. S., Costa, B., Gouveia, M. J., & Ferreira, A. (2020). Cell-penetrating peptides in oncologic pharmacotherapy: A review. *Pharmacological Research*, *162*(August).

Vergoni, A. V., Tosi, G., Tacchi, R., Vandelli, M. A., Bertolini, A., & Costantino, L. (2009). Nanoparticles as drug delivery agents specific for CNS: in vivo biodistribution. *Nanomedicine: Nanotechnology, Biology, and Medicine*, *5*(4), 369–377.

Wahajuddin, & Arora, S. (2012). Superparamagnetic iron oxide nanoparticles: Magnetic nanoplatforms as drug carriers. *International Journal of Nanomedicine*, *7*, 3445–3471.

Wallyn, J., Anton, N., & Vandamme, T. F. (2019). Synthesis, principles, and properties of magnetite nanoparticles for in vivo imaging applications—A review. *Pharmaceutics*, *11*(11), 1–29.

Weller, J., & Budson, A. (2018). Current understanding of Alzheimer's disease diagnosis and treatment. *F1000Research*, *7*(0), 1–9.

Wilhelm, I., Molnár, J., Fazakas, C., Haskó, J., & Krizbai, I. A. (2013). Role of the blood-brain barrier in the formation of brain metastases. *International Journal of Molecular Sciences*, *14*(1), 1383–1411.

Wolinsky, D., Drake, K., & Bostwick, J. (2018). Diagnosis and Management of Neuropsychiatric Symptoms in Alzheimer's Disease. *Current Psychiatry Reports*, *20*(12).

Xu, Z., Shen, C., Hou, Y., Gao, H., & Sun, S. (2009). Oleylamine as both reducing agent and stabilizer in a facile synthesis of magnetite nanoparticles. *Chemistry of Materials*, *21*(9), 1778–1780.

Yan, X., Bernard, J., & Ganachaud, F. (2021). Nanoprecipitation as a simple and straightforward process to create complex polymeric colloidal morphologies. *Advances in Colloid and Interface Science*, *294*(June), 102474.

Yavarpour-Bali, H., Pirzadeh, M., & Ghasemi-Kasman, M. (2019). Curcumin-loaded nanoparticles: A novel therapeutic strategy in treatment of central nervous system disorders. *International Journal of Nanomedicine*, *14*, 4449–4460.

Yoon, H. Y., Saravanakumar, G., Heo, R., Choi, S. H., Song, I. C., Han, M. H., Kim, K., Park, J. H., Choi, K., Kwon, I. C., & Park, K. (2012). Hydrotropic magnetic micelles for combined magnetic resonance imaging and cancer therapy. *Journal of Controlled Release*, *160*(3), 692–698.

Zhang, L., Chan, J. M., Gu, F. X., Rhee, J. W., Wang, A. Z., Radovic-Moreno, A. F., Alexis, F., Langer, R., & Farokhzad, O. C. (2008). Self-assembled lipid-polymer hybrid nanoparticles: A robust drug delivery platform. *ACS Nano*, *2*(8), 1696–1702.

Zhang, Z., Wang, X., Zhu, R., Wang, Y., Li, B., Ma, Y., & Yin, Y. (2016). Synthesis and characterization of serial random and block-copolymers based on lactide and glycolide. *Polymer Science - Series B*, *58*(6), 720–729.

Zheng, H., & Koo, E. H. (2006). The amyloid precursor protein: Beyond amyloid. *Molecular Neurodegeneration*, *1*(1), 1–12.

Zheng, T., Bott, S., & Huo, Q. (2016). Techniques for Accurate Sizing of Gold Nanoparticles Using Dynamic Light Scattering with Particular Application to Chemical and Biological Sensing Based on Aggregate Formation. *ACS Applied Materials and Interfaces*, *8*(33), 21585–21594.